

PARAMETERS INFLUENCING THE CORROSION PROTECTION
SERVICE LIFE OF EPOXY COATED REINFORCING STEEL IN
VIRGINIA BRIDGE DECKS

by

Megan C. Wheeler

Thesis submitted to the faculty of
Virginia Polytechnic Institute and State University
in partial fulfillment of the requirements for the degree of

Master of Science

in

Civil & Environmental Engineering

Committee Members

Richard E. Weyers, Chair
Christine Anderson-Cook
Michael C. Brown

December 9, 2003
Blacksburg, Virginia

**Keywords: epoxy coated reinforcing steel (ECR), bridge decks, corrosion, concrete,
glass transition temperature**

Copyright 2003, Megan C. Wheeler

PARAMETERS INFLUENCING THE CORROSION PROTECTION
SERVICE LIFE OF EPOXY COATED REINFORCING STEEL IN
VIRGINIA BRIDGE DECKS

Megan C. Wheeler

ABSTRACT

This study is an evaluation of epoxy coated reinforcing steel (ECR) and its ability to effectively provide corrosion protection in reinforced concrete highway bridge decks. An analysis was conducted on 10 bridge decks built in the state of Virginia between the years 1981 and 1995.

A total of 141 cores containing either ECR or bare steel were evaluated. A chloride solution was applied to the surface on a weekly cycle (for a total duration of 3.06 years) and a nondestructive electrochemical testing was performed on each core on a monthly cycle. Cores were also inspected for surface cracks, the thermal properties of the epoxy coating, and the concrete conditions at bar depth. The concrete was tested for saturation percentages, diffusion coefficients, and chloride contents, while the epoxy was tested for its glass transition temperature, moisture content, and amount of surface cracking.

The results indicate that the best predictor for estimating the times to corrosion initiation and cracking is the amount of chlorides present in the concrete encasing the ECR. The presence of chloride ions will have a determining effect on corrosion regardless of the epoxy coating condition. As a result, it is likely that ECR is not the solution to corrosion prevention and it is recommended that closer attention be given to improving concrete conditions that reduce the diffusion of chloride ions. The conclusion that ECR is an unreliable corrosion prevention method is in agreement with the results of previous studies.

TABLE OF CONTENTS

ABSTRACT	ii
TABLE OF CONTENTS	iii
LIST OF TABLES	v
LIST OF FIGURES	vi
INTRODUCTION	1
BACKGROUND	3
PURPOSE AND SCOPE	5
METHODS AND MATERIALS	6
<u>Field Procedure</u>	6
<u>Laboratory Testing</u>	6
<i>Core Preparation and Procedures</i>	6
<i>Specimen Preparation and Treatment for Electrochemical Testing</i>	6
<u>Physical Testing</u>	7
<i>Electrochemical Impedance Spectroscopy (EIS) Testing</i>	7
<i>Chloride Testing</i>	9
<i>Damage, Holidays, and Coating Thickness</i>	9
<i>Adhesion Loss Rating</i>	9
<i>Thermogravimetric Analysis (TGA)</i>	10
<i>Glass Transition Temperature (T_g)</i>	10
<i>Field Emission Scanning Electron Microscopy (FE-SEM)</i>	10
RESULTS	12
<u>Summary of Results Obtained from Previous Study</u>	12
<u>Continued Testing for Laboratory Core Evaluation</u>	12
<i>Chloride Concentration at Sampling and Cracking</i>	13
<i>Determining Corrosion Initiation</i>	17
<u>Additional Testing for ECR Samples</u>	22
<i>Description of ECR Specimen Selection Process for Additional Testing</i>	22
<i>Test Results Summary</i>	25
<i>Glass Transition Temperatures</i>	25
<i>Moisture Content of Epoxy Coating</i>	27
<i>Crack Frequency</i>	28
<i>Holidays</i>	28
<i>Thickness</i>	29
<i>Adhesion</i>	30
<i>Percent Saturation of Voids in Concrete at Bar Depth</i>	30
ANALYSIS AND DISCUSSION	31
<u>Section One: Continued Testing for Laboratory Core Evaluations</u>	31
<i>Time to Corrosion Initiation</i>	32
<i>Time to Corrosion-Induced Cracking</i>	33
<i>Propagation Time</i>	34
<i>Chloride at Bar Depth at Cracking</i>	35
<i>Estimating Chloride at Bar at Initiation</i>	37

<i>Summary and Significance for the Updated Results</i>	39
<u>Section Two: Testing of the Epoxy Coating</u>	40
<i>Initial T_g</i>	40
<i>Fully-Cured T_g</i>	41
<i>Change in T_g</i>	42
<i>Epoxy Moisture Content</i>	42
<i>Moisture Content versus Change in T_g</i>	43
<i>Crack Frequency and Crack Width</i>	43
<i>Cracking Frequency versus Change in T_g</i>	45
<u>Section Three: Determining Corrosion Initiation Time and Cracking Time from Epoxy and Concrete Parameters</u>	46
<i>Comparing Initiated, Non-Initiated, and Cracked Specimens</i>	46
<i>Parameters Influencing Time to Corrosion Initiation</i>	47
<i>Parameters Influencing Time to Corrosion-Induced Cracking</i>	49
CONCLUSIONS	51
RECOMMENDATIONS	52
ACKNOWLEDGEMENTS	53
REFERENCES	54
APPENDICES	55
(A) LITERATURE REVIEW	56
<u>Corrosion of Steel in Concrete</u>	56
<i>The Passive State</i>	56
<i>Mechanism for Bare Steel in Concrete</i>	56
<i>Chloride-Induced Corrosion</i>	57
<i>Corrosive Reactions of Reinforced Concrete Specimens</i>	57
<i>Chloride Corrosion Threshold</i>	57
<i>Summary of Corrosion Prevention Methods</i>	58
<u>ECR</u>	58
<i>Epoxy Polymers; an Overview</i>	58
<i>Manufacturing ECR</i>	59
<i>Glass Transition Temperature (T_g)</i>	59
<i>Characteristics of ECR as a Corrosion Prevention Method</i>	59
<i>Damage of ECR</i>	60
<i>Corrosion of ECR</i>	61
<u>Testing Methods</u>	62
<i>Electrochemical Impedance Spectroscopy</i>	62
<i>Differential Scanning Calorimetry</i>	64
<i>Thermogravimetric Analysis</i>	66
<i>Scanning Electron Microscopy</i>	66
LITERATURE REVIEW REFERENCES	68
VITA	71

LIST OF TABLES

Table 1	Adhesion Rating and Description	9
Table 2	Bridge Location, Identification, and Construction Details	12
Table 3	Core Status Summary	13
Table 4	Chloride Concentrations and Diffusion Coefficients – ECR	14
Table 5	Chloride Concentrations and Diffusion Coefficients – Bare Steel	17
Table 6	Initiation and Cracking Period – ECR	19
Table 7	Initiation and Cracking Period – Bare Steel	22
Table 8	Summary of ECR Samples Selected for Further Testing	23
Table 9	ECR Sample Selected for Testing from Previous Study	23
Table 10	ECR Samples Selected for Truncation and Testing from Present Study	24
Table 11	Cracked Samples Selected from Present Study	25
Table 12	ECR Data Summary for Percent Epoxy Moisture, T_g , and Crack Frequency from Previous Study Samples	26
Table 13	ECR Data Summary for Percent Epoxy Moisture from Present Study Samples	27
Table 14	ECR Data Summary for Epoxy Coating Thickness, Holidays, and Adhesion & Percent Concrete Void Saturation	29
Table 15	Summary of Average Time Periods for Chloride-Induced Corrosion Initiation, Cracking, and Propagation for Bare Steel and ECR	31
Table 16	Data Summary for Cracking and Concrete Parameters	47
Table 17	Correlation Matrix for Time to Corrosion Initiation	48
Table 18	Correlation Matrix for Time to Corrosion-Induced Cracking	50

LIST OF FIGURES

Figure 1	Designated Core Sections for Testing (side view)	7
Figure 2	Cell Connection Diagram for Electrochemical Testing	8
Figure 3	Example of a thermogram for an epoxy sample	11
Figure 4	Determining Time to Corrosion Initiation	18
Figure 5	T_g values for specimens from previous phase of study	26
Figure 6	Shelf Life versus % Epoxy Moisture Content	28
Figure 7	Typical Rating Results for Epoxy Surface Cracks from SEM Photographs	30
Figure 8	Corrosion Initiation Rate for Bare Steel and ECR	32
Figure 9	Corrosion-Induced Cracking Rate for Bare Steel and ECR	34
Figure 10	Histograms of Corrosion Propagation Periods for Bare Steel and ECR	35
Figure 11	Histograms of Chloride Concentrations at Bar Depth for Cracked and Truncated ECR Specimens	36
Figure 12	Histograms of Chloride Concentrations at Bar Depth at Cracking for Bare Steel and ECR Specimens	37
Figure 13	Estimate of Chloride Concentration at Bar Depth at Corrosion Initiation for Bare Steel and ECR	38
Figure 14	Histogram of Initial T_g Values	41
Figure 15	Histogram of Fully-Cured T_g Values	41
Figure 16	Histogram of Change in T_g Values	42
Figure 17	Histogram of (%) Epoxy Moisture Content	42
Figure 18	Epoxy Moisture versus Change in T_g	43
Figure 19	Histogram of Crack Frequency	44
Figure 20	SEM Photograph with 10K Magnification Showing Epoxy Crack Width Measurements	44
Figure 21	Crack Frequency versus Change in T_g	46
Figure 22	Time to Initiation versus Chlorides at Initiation	49
Figure 23	Time to Cracking versus Chlorides at Cracking	50
Figure 24	Schematic Representation of Polymers at (a) Linear, (b) Branched, and (c) Cross-linked (Networked) Stages	60
Figure 25	Electrochemical Impedance Spectroscopy Schematic Data Display for a Corroding Electrode by (a) Nyquist Plot and (b) Bode Plot	63
Figure 26	Schematic Representation of a Typical DSC System	64
Figure 27	Idealistic Thermogram	65
Figure 28	Temperature Transitions Measured by Noting Onset and Offset Points	66

INTRODUCTION

In recent decades it has become evident that U.S. highway bridge decks are deteriorating at an alarming rate. Concerns about this problem began to emerge in the 1960s when it was found that a growing number of U.S. highway bridge decks were in need of significant repairs, primarily due to corroding steel reinforcing bars, only a few years after their construction, (FHWA, 2002; Manning, 1996). The bridge deck deterioration tended to occur in areas of the country that also faced severe seasonal ice and snow and frequently used deicing salts on the pavement's surface to improve traffic conditions. By the 1970s, the problem of corroding reinforcing steel could be traced directly to deicing salts and their corrosive reaction on the metal's surface (FHWA, 2002). Ever since the appearance of this problem, conscious efforts have been made to improve the conditions of the deteriorating bridges through the intervention of corrosion prevention methods for reinforcing steel.

Increased attention for the overall quality of highway bridges has yielded improvements. According to the National Transportation Statistics Report for the year 2000, the percentage of rural and urban U.S. highway bridges that are considered to be structurally deficient has decreased from 24% to 14% between 1990 and 2000 (National Transportation Statistics 2000, 2001). However, regardless of the developments made in managing and constructing highway bridge decks, the amount of structurally deficient bridges continues to be relatively high, and transportation departments must continue to investigate both current and alternative methods for corrosion prevention. Unfortunately, it is not an option to eliminate the actual corrosive deicing salt source, mainly because of its benefit of improving motorists' safety and lack of an affordable, less problematic, alternative. Therefore, a reliable corrosion prevention method needs to be established that can be implemented in a cost effective manner. According to a recent report for the Federal Highway Administration (FHWA, 2002), the cost for annually repairing highway bridge corrosion damage in the U.S. is projected to be \$8.3 billion (Koch, 2002). Although a specific amount for bridge decks that are structurally deficient due to corrosion remains uncertain, it is evident that corrosion for steel reinforcing bars is one of the leading causes of overall bridge deck deterioration.

Thus far, the most widely adopted method for protecting reinforcing steel from corrosion is through the application of a fusion-bonded organic epoxy powder to coat the metal surface. The resultant product has been named Epoxy Coated Reinforcing bar (ECR) (Clifton, 1974). After conducting a study in the early 1970s, the FHWA recommended this material to the market as the most dependable method of protecting the steel. Since its introduction in West Conshohocken, Pennsylvania in 1973, ECR experienced increasing acceptance and has developed rapidly within the bridge construction industry, due to its relatively low construction cost, ease of application, and projection to significantly improve the service life for highway bridge structures. Presently, ECR has been in practice for highway agencies in 48 states and has been implemented in close to 95% of all highway bridges built from the early 1980s to present (FHWA, 2002).

Despite ECR's initial and continued acceptance as a protective barrier coating against corrosion, ongoing studies have been conducted that question the overall effectiveness of the material. As a result, investigations have produced conflicting evidence on its ability to perform successfully.

Potential problems were revealed soon after its introduction to the market when a study by the National Experimental and Evaluation Program found that ECR was destined to face damage during regular handling of the material at the construction sites. As a result, specifications were established promptly for ECR damage to measure less than 2% of the coating surface (FHWA, 2002; Manning, 1996). The FHWA presented evidence that even damaged ECR would possibly extend the service life by 46 years for highway bridges in comparison to black steel (Virmani, 1983). Based on this evidence, concerns about ECR's performance ability were assuaged, and ECR applications continued to be a regular practice in bridge construction.

Attitudes about ECR underwent a significant change in the late 1980s when the first serious indication of ECR's failure to effectively provide corrosion protection occurred (McKeel, 1977). Literature circulated that several bridges in the Florida Keys containing ECR in the substructure experienced severe corrosion only a few years after construction. Apparently, the steady exposure of marine salt water at the substructure portion of the bridge provided an ideal environment for corrosion development.

Subsequent studies revealed that if the epoxy coating is adhered properly to the steel's surface, it should be able to prevent corrosion. However, if an ECR coating contains surface damage, corrosion can occur in areas that have experienced adhesion loss and these areas are now as susceptible to corrosion as bare steel would be. Therefore, the question that needs to be investigated is the ability of epoxy to properly adhere to and protect the metal's surface, thereby providing a protective barrier against corrosion. Because this is the leading method used in preventing corrosion in highway bridge decks, a better understanding of the parameters involved with ECR corrosion needs to be established, so that U.S. transportation agencies can make informed decisions on the use of ECR in future highway bridge construction, compared to alternative methods.

BACKGROUND

Shortly after the initial introduction of ECR in 1973, the state of Virginia began using ECR as the prime method of corrosion protection for their highway bridge decks. Subsequently, field performance began to be conducted in Virginia in 1977, beginning with two ECR bridge decks, which were compared to two bridges containing bare steel (McKeel, 1977). Data were collected for each bridge and evaluated for the presence of chlorides and corrosion. The study found that there were no signs of active corrosion in the samples.

Since this initial field investigation, other studies by the Virginia Transportation Research Council (VTRC) yielded evidence contrary to the 1977 study. In 1996, three bridge decks and three marine structures containing ECR were investigated (Pyc, 1998). The results indicated that the epoxy coating is expected to experience adhesion loss from the steel surface due to water alone, before the arrival of chloride ions. If an epoxy coating becomes debonded from the reinforcing steel, it is not an effective chloride ion barrier. The corrosion process begins when an environment, containing moisture, oxygen, and other anions, is provided. Once the coating loses adhesion from ECR, its ability to provide proper corrosion protection is of no value and it becomes as vulnerable to corrosion as bare steel.

The results found in that study raised questions about ECR's ability to effectively protect the steel from corroding and prompted further research sponsored by the VTRC to investigate the performance of ECR. In particular, two consecutive studies were performed shortly after the 1996 investigation. Both reports contain data on ECR performance in selected bridge decks in Virginia and specific aspects of the data are highlighted in this study and used in an extended analysis found elsewhere in this paper.

The first study was conducted by Wioleta Pyc and Richard Weyers in 1997 and involved an analysis of ECR performance in 18 bridge decks built between 1987 and 1995 (Pyc, 1998). Approximately 12 cores were extracted from each bridge deck and examined for the coating's damage, adhesion, and thickness.

The main objective of Pyc's study was to estimate the amount of time it takes for an epoxy coating to lose adhesion from the steel reinforcing bar's surface. The findings for this research revealed that there was a loss of adhesion in ECR bridge decks in as little as four years and that the coating would undergo adhesion loss before the arrival of chloride ions. In addition, a close examination of the steel surface beneath the epoxy showed potential areas for corrosion development. The report concluded that ECR is not able to effectively prevent corrosion and it is only able to provide a minor extension of service life, if at all, when compared to bare steel reinforcement.

The second study, which used similar methods to those used by Pyc, was completed by Michael Brown and Richard Weyers in 2002. This research involved an analysis of concrete cores containing a single reinforcing steel bar for 2 bridge decks with bare steel and 8 containing ECR, built between 1981 and 1995 (Brown, 2002). All of the ECR

bridges were a subset from Pyc's 1997 study. Lab testing was conducted to monitor the corrosion level of each core and coincided with the application of a chloride solution on a weekly cycle for a total of 1.94 years. During this time period, nondestructive electrochemical impedance spectroscopy (EIS) testing, along with visual observations, were made for each core and the time of corrosion initiation and the time of corrosion-induced cracking were documented. Once a core showed visual evidence of cracking, it was removed from the ponding and testing cycle and was disassembled so that a detailed analysis could be made of the reinforcement and concrete.

At the end of the 1.94 year study, 27 out of the 28 bare steel bar cores and 21 of the 113 ECR cores cracked. In addition, 17 of the ECR cores were randomly selected and examined prior to cracking (truncated specimens). All applicable data concerning time to corrosion initiation, time to corrosion-induced cracking, and chloride content, for the total 141 specimens are summarized in the Results section of this report and all truncated cores are specified.

The primary purpose of Brown's study was to establish an estimation of the extended service life for ECR when compared to bare steel. The service life for ECR was approximated by measuring the amount of time it took for a specimen to crack once corrosion initiation had taken place. The study reports that the amount of time for bridge deck service life that ECR is able to extend beyond that of bare steel is about 5 years.

The results from these studies reveal information that is far from the initial claims made during the introduction of ECR in the 1970s, when it was originally estimated to extend the service life 46 years in comparison to using bare steel (FHWA, 2002). As a result, Brown's investigation was continued in the present study, which involves enhanced testing of the epoxy coating in an effort to establish the parameters that influence corrosion.

PURPOSE AND SCOPE

This research continues a previous study so that a more in-depth analysis can be conducted on the remaining cores (Brown, 2002). The additional data may be useful in establishing a better estimate of the time to corrosion-induced cracking for ECR.

The objective of this study is to identify the parameters that influence corrosion initiation and cracking for ECR in relation to coating and concrete conditions. This study also serves to evaluate epoxy coatings and their ability to effectively provide corrosion protection.

Collectively, the goal of this research is to present informative data on ECR performance and to offer guidance for Virginia transportation agencies to make knowledgeable decisions when selecting methods for corrosion prevention.

The range of information accumulated in this study is limited to a total of 141 concrete core specimens from 10 Virginia highway bridge decks, 8 containing ECR and 2 containing bare steel. The level of corrosion was monitored for a total of 3.06 years, coinciding with chloride solution application on a weekly cycle. Experimental data was collected on corrosion initiation while visual observations were made on specimens for cracking. Upon specimen cracking, further analysis was made on coating and concrete properties as a guide in assessing the ECR parameters associated with chloride-induced cracking.

At present, all 28 bare steel cores, along with 25 of 113 ECR cores, have cracked and 47 ECR cores have been tested before cracking occurred. The corrosion status of all cores was monitored throughout the duration of the study. All cracked and truncated specimens were autopsied for further testing of coating conditions and concrete chloride content. Of the failed and truncated specimens, 54 were selected for additional testing to assess a more detailed analysis of the epoxy coating.

METHODS AND MATERIALS

This section begins with a review of testing procedures conducted by Pyc and Brown in 1997 and 2002, in an effort to explain how the data discussed in the Background section of this report was obtained. The following testing procedures were also applied to selected specimens for the present study, where applicable.

Field Procedure

In Brown's study, cores were extracted from 8 bridge decks containing ECR that were also used in Pyc's study and 2 decks containing bare steel. The 8 ECR bridge decks were carefully selected so that a variety of adhesion loss levels were represented. The 2 bare steel bridge decks were used for comparison. For Brown's study, a total of 141 102mm diameter cores were obtained. Each bridge deck was represented by 10 to 12 cores and contained a top reinforcing bar. Locations were adjacent to cores extracted in Pyc's study. Also, 3 additional cores were taken in each bridge deck at surface crack locations. The cores selected from all 10 bridge decks were from the 12 percentile smallest clear concrete cover depth.

Laboratory Testing

Core Preparation and Procedures

Each core was prepared for testing so that designated sections could be reserved for measuring the chloride content, water absorption, and moisture content, while the remainder of the core was used for electrochemical testing of corrosion conditions. A diagram is labeled in Figure 1 for a typical core sectioning format used. Two sections of the core were used for measuring the chloride content while two other sections were used to measure moisture content, percent absorption, and percent saturation. One section was located 13 mm below the pavement surface and the other at 13 mm above the reinforcing steel. Collectively, these values were used for analysis in Brown's study.

Specimen Preparation and Treatment for Electrochemical Testing

Sections of each core measuring approximately 83 mm in length were reserved for EIS testing. Preparation for EIS testing involved drilling and tapping for a stainless steel screw to be inserted into one side of the reinforcement steel of each core, which was used as a connection to the EIS equipment. The outer and bottom surfaces of each core were coated with paraffin wax to serve as a moisture barrier, while the top surface remained uncovered for application of a 3% NaCl ponding solution that was applied on a weekly basis for a period of 2 to 4 days. The ponding solution was held by a reservoir device consisting of a 76 mm PVC pipe section and was attached to the surface of the core with a silicone sealant. Each core was tested at 4-week increments.

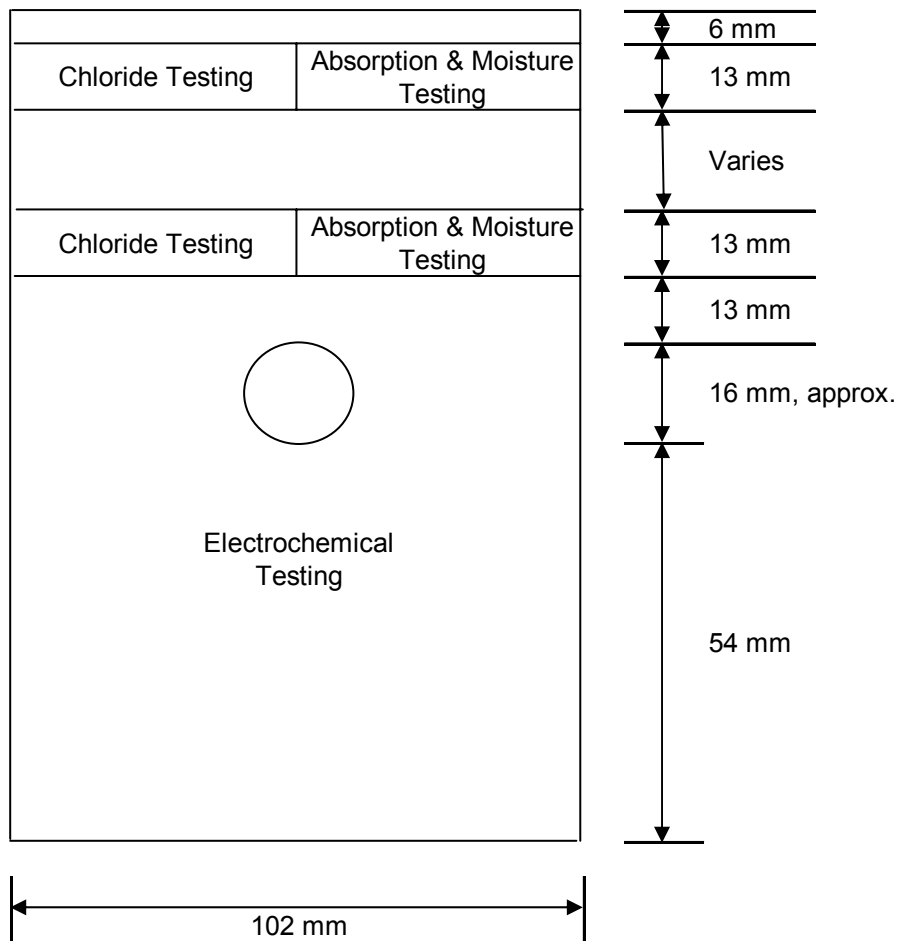


Figure 1 Designated Core Sections for Testing (side view)

Physical Testing

Electrochemical Impedance Spectroscopy (EIS) Testing

Testing consisted of measurements made with a computer-controlled potentiostat system. EIS is a process that monitors the relationship of the conductivity conditions and the metal surface. This is performed by applying an alternating potential to the reinforcement that is relative to a reference electrode (Cu-Cu(SO₄)). The current and the potential values are measured and are used to calculate impedance.

The EIS testing methods were supplied by Gamry Instruments Framework software and pertinent data for analysis were consolidated into spreadsheets. The equipment used for electrochemical testing involved probes that were uniquely manufactured, with a 73mm diameter counter-electrode consisting of titanium mesh embedded in a sponge. Surface contact for the probe was secured by a concrete weight and the probe accommodated a

pen-cell type reference electrode half-cell. Figure 2 provides a model for the cell connection locations in relation to the concrete core specimen.

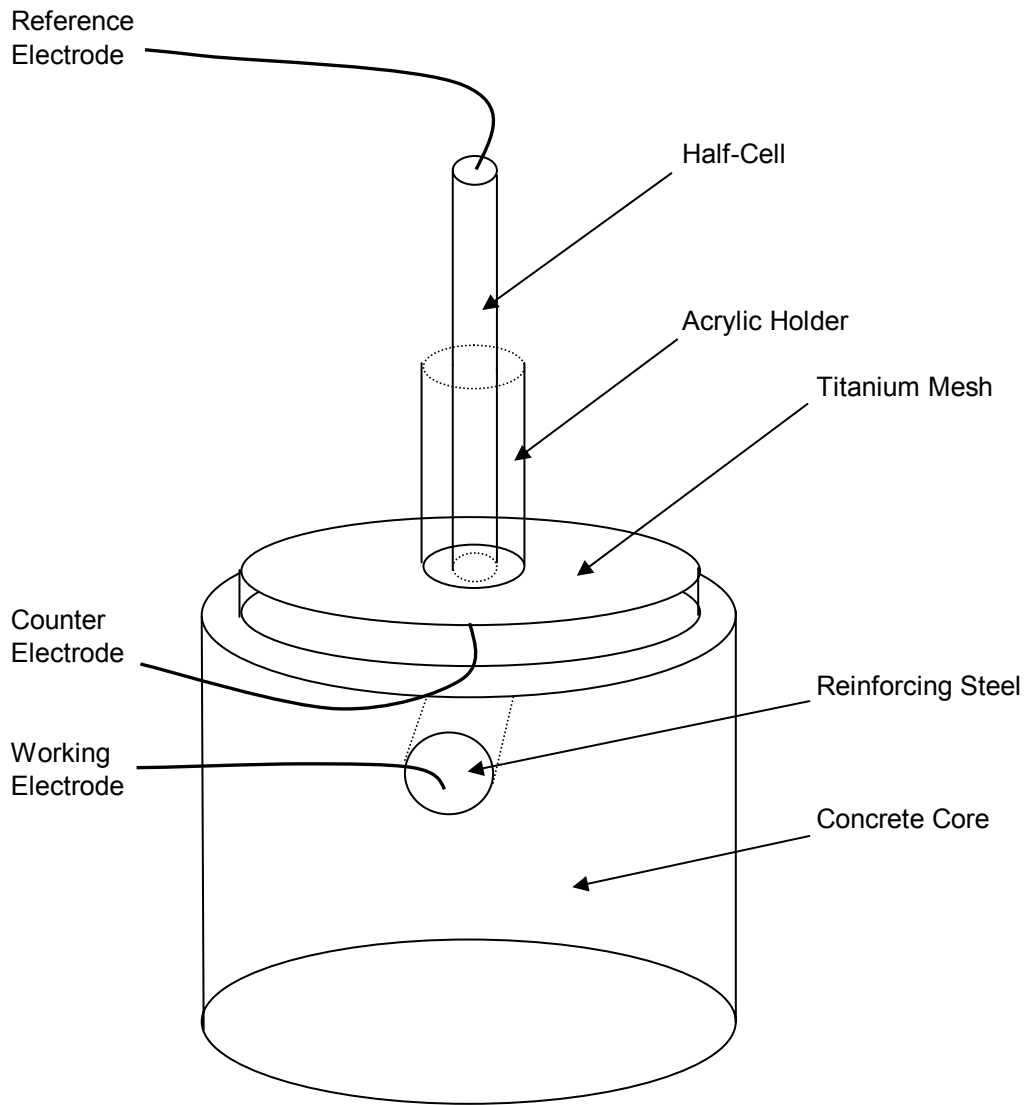


Figure 2 Cell Connection Diagram for Electrochemical Testing

Testing for EIS was conducted with a frequency sweep that varied between 0.001 Hertz to 5000 Hertz and had an amplitude of ± 10 mV from the open-circuit corrosion potential. Data were acquired and presented graphically by Bode and Nyquist plots. Bode plots provided the modulus of impedance, along with values for the phase angle versus the frequency. Nyquist plots present the real impedance versus the imaginary impedance. Simplistically, a frequency of 0.001 Hz generates impedance values of both the electrolyte and ECR, while a frequency of 5000 Hz produce impedance values of just the

concrete electrolyte. Collectively, these plots containing both potential and impedance data, provided the information necessary for analysis of time to corrosion initiation.

Chloride Testing

Designated sections of the core were reserved for chloride analysis. Each sample was prepared for a chemical analysis by manually crushing the concrete into a powder until it was fine enough to pass through a No. 20 sieve. Samples were measured at approximately 10.0g and tested by an acid-soluble chloride concentration test, in agreement with a procedure outlined by ASTM C 1152-90. The values obtained from chloride testing were used to determine the chloride concentration for the concrete that was adjacent to areas of the reinforcement undergoing active corrosion.

Holidays and Coating Thickness

Once the ECR was removed from a core, holidays were detected, in accordance with ASTM G 62, to identify an approximate amount of flaws in the ECR coating. In addition, measurements were made on the coating thickness utilizing a Minitest 500 coating thickness gauge.

Adhesion Loss Rating

Adhesion loss for all autopsied ECR samples was determined through a knife adhesion test. The testing procedure involved cutting an “x” on the epoxy surface followed by inserting an ex-acto knife beneath the coating surface. Adhesion was measured on a scale of 1 to 5 and the description for each adhesion value is outlined in Table 1.

Table 1 Adhesion Rating and Description

Adhesion Number	Description
1	not able to remove coating with blade tip
2	visible steel is <2mm ²
3	visible steel is >2mm ² and <4mm ²
4	visible steel is >4mm ²
5	blade tip easily slides beneath coating and removes entire testing section

Thermo Gravimetric Analysis (TGA)

The moisture content for the epoxy coating was acquired using a TGA device that heats a specimen and measures weight versus temperature over time for a given sample. Moisture content is measured by the amount the weight decreases from moisture loss at elevated temperatures beyond the boiling point of water.

Samples of epoxy weighing approximately 4.0g were used for moisture content measurements. The temperature was raised to 150.00°C and held in equilibrium for 20 minutes to ensure all moisture was extracted from the sample.

Glass Transition Temperature (T_g)

The glass transition temperature (T_g) was measured for 4.0g epoxy samples through use of a Differential Scanning Calorimeter (DSC) system. DSC measures the T_g of a sample using thermogram plots, which monitors an epoxy's energy level (the amount of heat the polymer absorbs or emits per unit mass) as a function of temperature. A more detailed discussion for interpreting a DSC thermogram is offered in the Literature Review section of this paper.

To measure the T_g , the DSC was programmed to equilibrate the temperature at 60.00°C and then increase the temperature at 10.00°C/min to 120.00°C. An example for how the T_g was interpreted from a DSC thermogram is provided in Figure 3, where the epoxy's heat energy index is monitored and plotted as a function of temperature. As seen on the plot, the T_g takes place at approximately 69.45°C where there is an increase in slope as more heat energy is required to break the substance down from its glass-like structure to its rubber state. Another observation that can be made on the thermogram example for Figure 3 is that additional curing is taking place as temperatures continue to be elevated. Additional curing is noted by a curing exotherm where energy is released as reactions take place as the epoxy polymer network continues to develop.

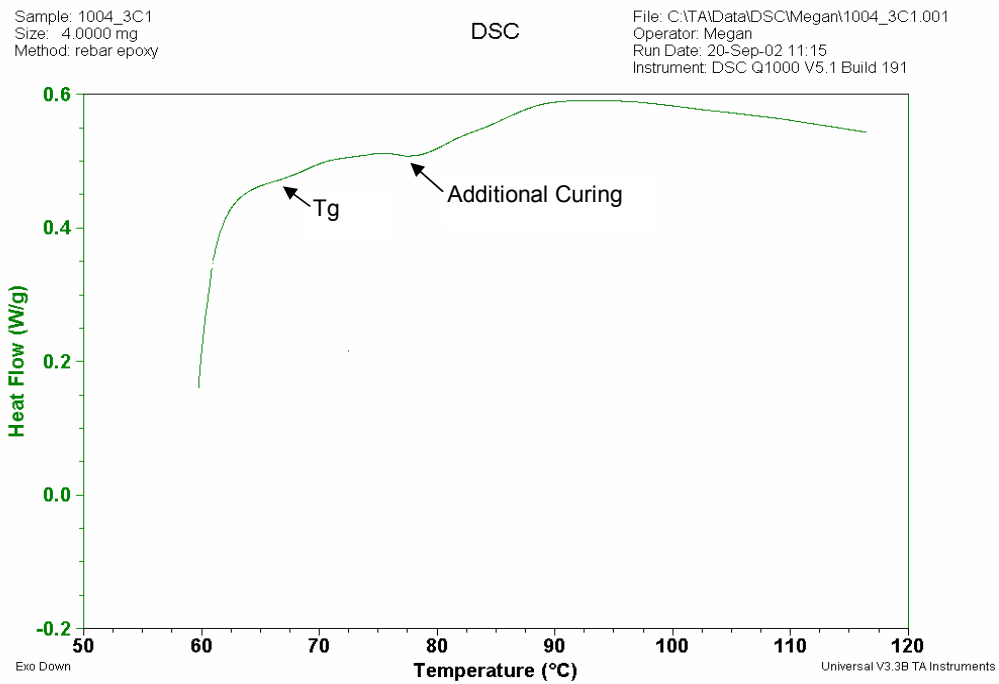
Once it had been determined that the samples had not been fully-cured, additional testing was conducted on each of the samples to determine its fully-cured T_g value. Prior to DSC testing, the samples were placed in an oven for 4 hours at 160.00°C to ensure enough time to become fully-cured. Next, the DSC was programmed to equilibrate at 80.00°C and temperatures were elevated at 10.00°C/min to 160.00°C. The values for each tested specimen's T_g and respective fully-cured T_g are presented in the Results section of this document.

Field Emission Scanning Electron Microscope (FE-SEM)

Enhanced images of the epoxy coating for ECR were taken using a LEO 1550 FE-SEM at 5kV. Photos were taken at magnitudes of 500, 2K, 10K, and 20K. The condition of the epoxy surface was examined for evidence of cracking. Particular attention was focused on observing both the crack width and the crack frequency, when applicable. The chemical composition for all images was evaluated by using Energy Dispersive

Spectroscopy (EDS) and was performed by an Iridium Microanalysis (I/RF) System. Typical elements detected for the epoxy coating included high concentrations of oxygen, sodium, and chlorine, along with traces of aluminum, magnesium, silicon, calcium, titanium, and chromium. The concrete was distinguished from the epoxy coating by much higher concentrations of silicon and calcium, while the steel was noted by high concentrations of iron and carbon.

Figure 3 Example of a thermogram for an epoxy sample



RESULTS

Summary of Results Obtained from Previous Study

This section presents a summary of pertinent data that has been collected from the preceding studies conducted by Pyc and Brown (Brown, 2002; Pyc, 1998). Table 2 displays information on the bridge location, age at time of sampling, the total number of cores that were extracted from each bridge deck, along with information on the bridge spans and reinforcing steel type. The bridges were constructed between the years 1981 and 1995, yielding bridges that ranged between 4 to 18 years old when the surveying took place. The dominant designs for the superstructure of each bridge were simply supported and continuous steel girder systems that included a composite deck formation (Brown, 2002). Only one bridge was constructed with prestressed concrete I-beams with continuous span. Eight of the bridges were built with ECR and two were constructed with bare steel.

Table 2 Bridge Location, Identification, and Construction Details

Bridge	District/County/Route	Year Built	Age	Total Cores	Spans	Span Lengths (m)	Structure Type	Reinforcement
1001	7/Culpeper/US 29	1992	7	14	3	23/23/24	S/C	ECR
1004_3	3/Nelson/SR 6	1983	16	14	3	18/18/19	S/C	ECR
1004_6	6/Northumberland/SR 200	1993	6	13	3	13/13/27	PI/C	ECR
1015	2/Giles/SR 100	1987	12	14	3	15/24/15	S/S	ECR
1019	7/Culpeper/US 522	1990	9	13	3	15/26/15	S/S	ECR
1136	1/Wise/SR 72	1995	4	15	3	22/22/22	S/C	ECR
2021	5/Greensville/I-95	1981	18	15	3	21/21/21	S/C	ECR
2262	9/Fairfax/Vaden Drive	1985	14	15	4	21/20/25/23	S/S	ECR
6037	1/Grayson/County 662	1983	16	12	2	20/20	S/S	BS
6128	2/Franklin/County 740	1984	15	16	2	17/17	S/S	BS

S/S - steel girders/simple supported
 PI/C - prestressed I-beams/continuous design
 S/C - steel girders/continuous design
 ECR - epoxy coated reinforcement
 BS - bare steel

Table 3 presents a summary of the final status for the 141 cores represented in this study.

Continued Testing for Laboratory Core Evaluations

All remaining cores from the previous phase of this study continued to be monitored for indication of corrosion initiation and measurements for concrete percent saturation, and chloride concentration were taken once the ponding process was complete. The updated version of results obtained from measuring the chloride concentrations, along with the time to corrosion initiation, propagation, and corrosion-induced cracking, are summarized in Tables 4 through 7. All new data collected in the present study is indicated by boldface print and truncated specimens from Brown’s study are marked by an “^”, while truncated specimens in the present study are marked by an “*”.

Table 3 Core Status Summary

Core Classification		Previous Study	Present Study	Sub Total (to date)	Total (to date)
Autopsied Cores	Cracked ECR	21	4	25	100
	Cracked (Bare Steel)	27	1	28	
	Truncated ECR (Initiated Corrosion)	9	15	24	
	Truncated ECR (Not Initiated)	8	15	23	
Remaining Cores	Initiated Corrosion	21	7	28	41
	Not Initiated	13	-	13	

Chloride Concentration at Sampling and Cracking

The chloride concentration was determined at two locations (identified in Figure 1 of document) for each core prior to laboratory testing during the previous study. Once a specimen had either cracked or had been selected for truncation, additional testing was conducted at selected locations directly above the bar's surface and directly adjacent to the bar. Also included in this section are values obtained for the effective chloride diffusion coefficient and estimated chloride at bar depth at the time of corrosion initiation. The diffusion coefficients and chlorides at initiation were estimated using Fick's 2nd law, which may be used to model the rate that chlorides ingress into the concrete. A solution to Fick's 2nd is as follows (Rieger, P.H., 1994):

$$C_{(x,t)} = C_o \{ 1 - \text{erf } x / (2(D_c t)^{1/2}) \} \quad \text{Equation 1}$$

where

$C_{(x,t)}$ = chloride concentration at depth, x and chloride exposure time, t

C_o = chloride concentration near the surface

D_c = effective diffusion coefficient

erf = error function

Table 4 for ECR and Table 5 for bare steel provide an updated summary for all chloride concentration values and diffusion coefficients that were determined after the ponding process was complete. Please note that all values obtained during the present study are highlighted by boldface print.

Table 4 Chloride Concentrations - ECR

* Specimens truncated prior to cracking from present study

^ Specimens truncated prior to cracking from previous study

Specimen	Before Lab Treatment		After Lab Treatment		Dc (mm ² /yr)	Initiation C(x,t) (kg/m ³)
	Cl at 12mm below surface (kg/m ³)	Cl at 19mm above the bar (kg/m ³)	Ave. Cl at bar depth (kg/m ³)	Ave. Cl above bar (kg/m ³)		
	1001_C1	1.78	0.00	-		
1001_C2	2.38	0.00	10.87	9.05	-	-
1001_C3*	1.99	0.07	21.45	14.47	-	-
1001_C4	1.84	0.00	-	-	-	-
1001_C5*	2.06	0.21	9.53	15.86	96	-
1001_C6*	2.74	0.91	8.82	16.14	72	-
1001_C7*	2.81	0.00	8.26	17.65	51	-
1001_C8	2.81	0.64	-	-	-	-
1001_C9	2.21	0.00	-	-	-	-
1001_C11	2.29	0.00	-	-	-	-
1001_C12	2.35	0.00	-	-	-	-
1001_CR1	1.93	1.18	-	-	-	-
1001_CR2	2.00	0.75	-	-	-	-
1001_CR3*	1.83	0.00	6.47	6.49	34745	-
1004_3_C1	2.97	1.18	9.60	6.85	-	-
1004_3_C2*	4.11	0.44	12.77	20.27	145	4.36
1004_3_C3	3.71	0.21	9.78	7.21	-	-
1004_3_C4	3.52	0.40	-	-	-	-
1004_3_C5	4.99	0.90	-	-	-	-
1004_3_C6*	3.58	0.56	10.85	9.81	-	-
1004_3_C7*	3.87	0.40	13.14	14.04	3861	-
1004_3_C8	4.34	0.22	-	-	-	-
1004_3_C9^	3.97	0.70	10.26	6.58	-	-
1004_3_C10	3.88	0.44	-	-	-	-
1004_3_C11*	4.73	1.68	9.66	9.58	-	-
1004_3_C12	3.66	1.18	8.82	11.45	410	7.16
1004_3_CR2	3.87	0.00	-	-	-	-
1004_3_CR3	4.42	0.00	-	-	-	-
1004_6_C1	0.74	0.00	-	-	-	-
1004_6_C2	0.94	0.00	-	-	-	-
1004_6_C3^	0.62	0.00	10.36	9.97	-	-
1004_6_C4*	0.88	0.00	11.83	15.10	347	-
1004_6_C5*	1.06	0.00	9.04	8.67	-	-
1004_6_C6	0.55	0.00	-	-	-	-
1004_6_C7	1.31	0.16	9.52	14.16	253	0.74
1004_6_C8^	0.74	0.00	9.14	13.67	263	-
1004_6_C10*	0.69	0.00	10.82	12.85	543	-
1004_6_C12^	0.79	0.00	12.93	13.48	28110	-
1004_6_CR1	0.79	0.20	-	-	-	-
1004_6_CR2	1.23	0.36	6.30	11.30	235	1.92
1004_6_CR3/C11	0.75	0.50	6.38	6.27	-	-

Table 4 Chloride Concentrations - ECR (continued)

Specimen	Before Lab Treatment		After Lab Treatment		Dc (mm ² /yr)	Initiation C(x,t) (kg/m ³)
	Cl ⁻ at 12mm below surface (kg/m ³)	Cl ⁻ at 19mm above the bar (kg/m ³)	Ave. Cl ⁻ at bar depth (kg/m ³)	Ave. Cl ⁻ above bar (kg/m ³)		
1015_C1	3.78	0.54	9.96	16.83	158	8.48
1015_C2*	3.05	1.16	12.39	14.23	1716	12.33
1015_C3	4.92	1.82	8.46	11.32	392	6.05
1015_C4^	6.17	3.07	9.50	12.00	701	9.07
1015_C5*	5.86	2.98	11.67	11.41	-	-
1015_C6	4.80	2.90	9.74	16.75	91	0.84
1015_C7*	5.81	1.17	14.46	17.51	543	3.80
1015_C8	5.72	1.86	9.30	14.35	192	0.71
1015_C9^	5.06	2.84	9.84	8.37	-	-
1015_C10	4.79	3.49	13.18	12.54	2071	8.46
1015_CR1^	4.42	3.67	7.40	9.98	478	5.13
1015_CR2	7.08	0.99	-	-	-	-
1015_CR3	4.50	0.48	10.95	15.99	270	1.13
1015_CR1B	2.76	0.41	10.72	12.97	793	3.59
1019_C1	1.67	0.10	-	-	-	-
1019_C2*	2.11	0.02	15.26	13.47	-	-
1019_C3*	1.25	0.01	14.26	11.18	-	-
1019_C4	2.34	0.07	-	-	-	-
1019_C5*	1.51	0.07	15.29	10.36	-	-
1019_C6*	2.90	0.24	17.65	12.73	-	-
1019_C7	1.96	0.17	-	-	-	-
1019_C8*	2.48	0.45	11.50	12.17	5559	-
1019_C9	2.19	0.29	-	-	-	-
1019_C10*	2.00	0.28	14.85	17.30	822	14.22
1019_CR1	1.26	0.47	-	-	-	-
1019_CR2^	1.53	0.76	10.22	12.53	112	4.55
1019_CR3	2.27	0.76	6.71	6.76	36260	6.55
1136_C1	4.19	0.03	-	-	-	-
1136_C2^	6.79	0.08	10.64	2.90	-	-
1136_C3*	7.17	0.35	7.78	3.30	-	-
1136_C4	5.81	0.04	-	-	-	-
1136_C5	2.85	0.00	-	-	-	-
1136_C6	3.62	0.00	-	-	-	-
1136_C7	3.25	0.04	7.73	15.92	108	0.08
1136_C8^	4.09	0.00	5.29	16.35	-	-
1136_C9	4.62	0.00	-	-	-	-
1136_C10*	3.78	0.00	2.60	4.64	-	-
1136_C11^	3.27	0.00	10.99	3.39	-	-
1136_C12	4.84	0.00	18.41	22.62	522	12.68
1136_CR1	7.29	0.16	-	-	-	-
1136_CR2	5.83	0.17	11.32	10.41	-	-
1136_CR3	5.41	0.33	7.92	13.17	-	-

Table 4 Chloride Concentrations - ECR (continued)

Specimen	Before Lab Treatment		After Lab Treatment		Dc (mm ² /yr)	Initiation C(x,t) (kg/m ³)
	Cl ⁻ at 12mm below surface (kg/m ³)	Cl ⁻ at 19mm above the bar (kg/m ³)	Ave. Cl ⁻ at bar depth (kg/m ³)	Ave. Cl ⁻ above bar (kg/m ³)		
2021_C1	0.60	0.06	-	-	-	-
2021_C2*	0.84	0.04	13.62	12.91	-	-
2021_C3*	0.72	0.00	9.47	13.23	206	6.58
2021_C4^	0.79	0.08	11.74	13.40	2091	-
2021_C5	0.60	0.45	-	-	-	-
2021_C6	1.09	0.52	6.29	8.83	591	1.79
2021_C7	1.60	0.67	-	-	-	-
2021_C8^	0.36	0.02	5.25	6.93	523	-
2021_C9*	0.76	0.01	15.39	10.21	-	-
2021_C10	1.03	0.00	-	-	-	-
2021_C11	1.23	0.53	-	-	-	-
2021_C12*	1.22	0.00	10.40	12.91	429	9.21
2021_CR1	0.56	0.04	6.33	12.35	190	4.53
2021_CR2^	0.34	0.20	12.18	5.66	-	-
2021_CR3*	0.60	0.00	8.41	11.15	263	-
2262_C1	2.61	1.30	-	-	-	-
2262_C2^	2.46	1.47	12.36	9.45	-	-
2262_C3	2.07	0.60	-	-	-	-
2262_C4	2.26	1.01	9.43	8.27	-	-
2262_C5	1.91	1.08	-	-	-	-
2262_C6	3.63	2.19	-	-	-	-
2262_C7^	1.34	0.23	11.61	5.36	-	-
2262_C8	1.87	0.91	10.48	9.50	-	-
2262_C9	1.46	0.88	-	-	-	-
2262_C10	0.67	0.50	9.85	10.17	8511	9.31
2262_C11^	1.20	0.07	7.42	-	-	-
2262_C12	2.33	0.00	-	-	-	-
2262_CR1*	0.24	3.43	11.46	7.07	-	-
2262_CR2	0.35	0.39	10.02	6.35	-	-
2262_CR3*	3.13	0.20	12.81	6.96	-	-

Table 5 Chloride Concentrations - Bare Steel

Specimen	Before Lab Treatment		After Lab Treatment		Dc (mm ² /yr)	Initiation C(x,t) (kg/m ³)
	Cl ⁻ at 12mm below surface (kg/m ³)	Cl ⁻ at 19mm above the bar (kg/m ³)	Ave. Cl ⁻ at bar depth (kg/m ³)	Ave. Cl ⁻ above bar (kg/m ³)		
6037_C1	0.83	-	2.23	12.72	74	0.01
6037_C2	0.74	-	4.88	10.14	252	0.41
6037_C3	0.78	-	7.93	15.27	138	0.89
6037_C5	0.00	-	7.23	10.93	170	0.14
6037_C7	0.14	0.00	7.10	15.67	105	2.95
6037_C8	0.76	0.21	3.42	6.87	275	0.39
6037_C9	0.34	0.14	8.18	14.20	158	5.84
6037_C10	0.16	0.63	14.91	18.38	517	10.00
6037_C11	0.78	-	5.69	14.40	156	0.19
6037_C12	0.18	0.06	13.39	18.12	401	9.08
6037_CR1/C4	0.44	0.23	7.76	19.06	71	0.01
6037_CR2/C6	0.34	0.25	9.50	14.96	256	0.79
6128_C1	0.15	0.00	12.42	16.01	725	3.35
6128_C2	0.17	0.00	8.42	14.82	247	0.46
6128_C3	0.15	0.00	4.98	8.56	292	2.54
6128_C4	0.25	0.00	7.09	10.95	426	1.11
6128_C5	0.00	0.00	8.09	7.35	-	-
6128_C6	0.09	0.02	4.39	13.65	127	1.55
6128_C7	0.08	0.06	6.48	9.54	514	3.18
6128_C8	0.16	0.02	9.04	14.66	235	0.40
6128_C9	0.15	0.02	6.98	11.26	392	2.97
6128_C10	0.12	0.10	7.42	14.32	210	1.90
6128_C11	0.13	0.01	6.38	7.09	6191	6.26
6128_C12	0.10	0.05	8.91	10.72	1285	3.82
6128_CR1	0.15	0.00	3.91	5.35	818	1.27
6128_CR2	0.11	0.13	6.41	7.60	2761	3.88
6128_CR3	0.31	0.20	5.54	6.65	1509	2.76
6128_CR4	0.20	0.04	8.03	6.03	-	-

Determining Corrosion Initiation

Active corrosion was observed to take place for both bare steel and ECR specimens that reached potential values that were more negative than -350mV CSE, which is in accordance to ASTM C876 standards for bare steel (ASTM, 1991). For ECR, an observed decrease in impedance must be consistent with a decrease in potential. The decrease in impedance was determined at 1 mHz because it was indicative of both the coating and corrosion variables. In addition to the impedance, the 1 mHz graph also plots the corresponding phase angle value, which has a direct relationship to the impedance. Discussion for the relationship between the phase angle and impedance values is discussed further in the Literature Review section of this document. Examples for determining the time to corrosion initiation for bare steel and ECR are shown on Figure 4 for the potential trends and impedance trends at 1 mHz. Tables 6 and 7 present time to corrosion initiation, propagation, and cracking data for ECR and bare steel, respectively.

Figure 4 Time to Corrosion Initiation is marked at 28 months

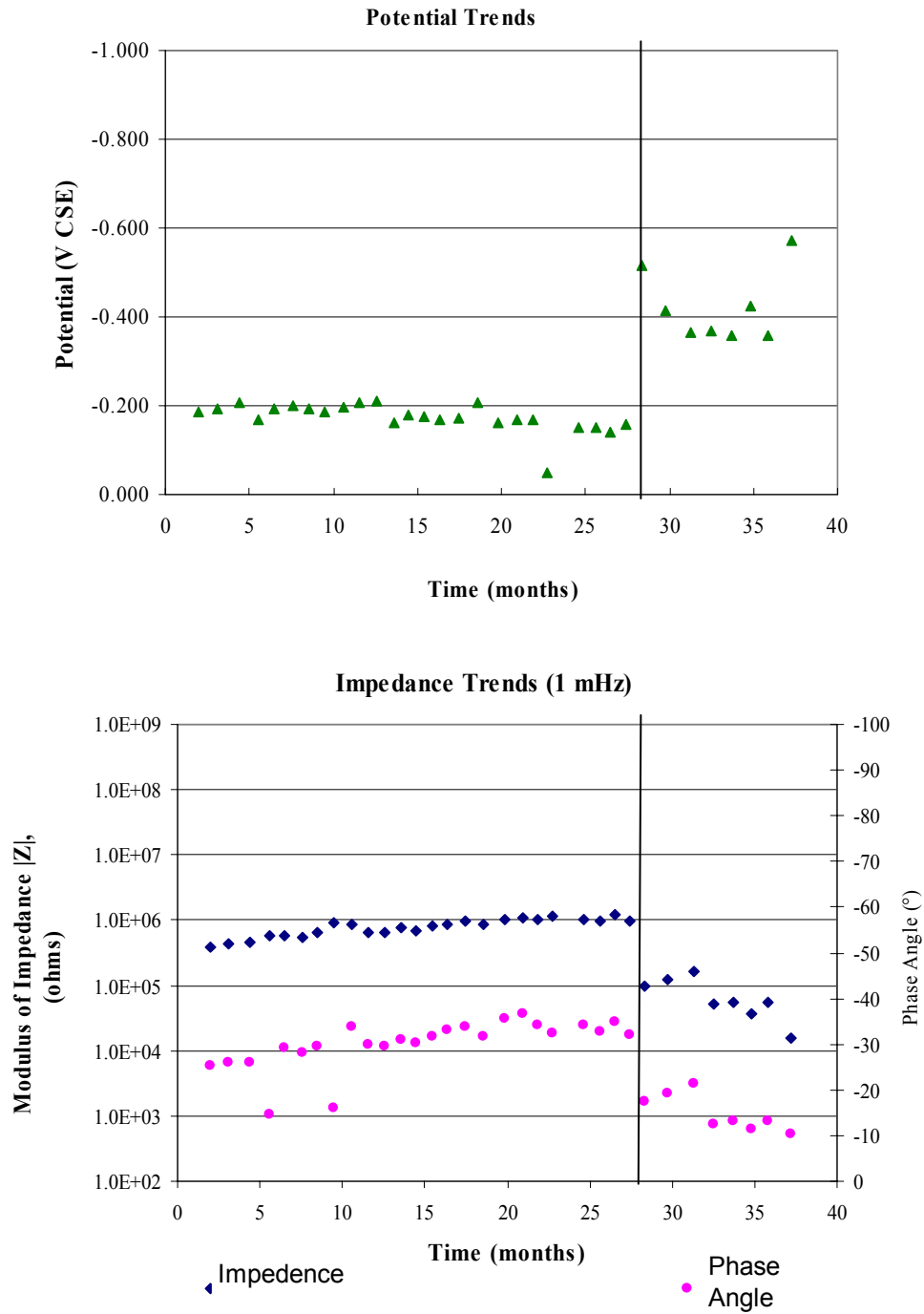


Table 6 Initiation and Cracking Period - ECR

* Specimens truncated prior to cracking from present study

^ Specimens truncated prior to cracking from previous study

Specimen	Time to Initiation (yrs)	Time to Cracking (yrs)	Propagation time (yrs)
1001_C1	-	-	-
1001_C2	0.90	1.89	0.99
1001_C3*	-	-	-
1001_C4	3.05	-	-
1001_C5*	-	-	-
1001_C6*	-	-	-
1001_C7*	-	-	-
1001_C8	2.58	-	-
1001_C9	-	-	-
1001_C11	-	-	-
1001_C12	0.18	-	-
1001_CR1	0.18	-	-
1001_CR2	-	-	-
1001_CR3*	-	-	-
<hr/>			
1004_3_C1	0.18	1.93	1.75
1004_3_C2*	0.38	-	-
1004_3_C3	0.81	1.93	1.12
1004_3_C4	1.92	-	-
1004_3_C5	0.81	-	-
1004_3_C6*	-	-	-
1004_3_C7*	-	-	-
1004_3_C8	-	-	-
1004_3_C9^	0.57	-	-
1004_3_C10	0.27	-	-
1004_3_C11*	0.18	-	-
1004_3_C12	0.72	1.83	1.11
1004_3_CR2	1.83	-	-
1004_3_CR3	0.57	-	-
<hr/>			
1004_6_C1	3.06	-	-
1004_6_C2	1.57	-	-
1004_6_C3^	-	-	-
1004_6_C4*	-	-	-
1004_6_C5*	2.58	-	-
1004_6_C6	2.67	-	-
1004_6_C7	0.09	1.86	1.78
1004_6_C8^	-	-	-
1004_6_C10*	-	-	-
1004_6_C12^	-	-	-
1004_6_CR1	1.74	-	-
1004_6_CR2	0.18	1.02	0.85
1004_6_CR3/C11	0.55	1.02	0.48

Table 6 Initiation and Cracking Period - ECR (continued)

Specimen	Time to Initiation (yrs)	Time to Cracking (yrs)	Propagation time (yrs)
1015_C1	1.18	1.85	0.67
1015_C2*	1.18	-	-
1015_C3	0.48	2.04	1.56
1015_C4^	1.30	-	-
1015_C5*	0.57	-	-
1015_C6	0.09	3.04	2.95
1015_C7*	0.10	-	-
1015_C8	0.10	1.91	1.81
1015_C9^	0.09	-	-
1015_C10	0.09	1.94	1.85
1015_CR1^	0.09	-	-
1015_CR2	0.09	-	-
1015_CR3	0.09	1.85	1.76
1015_CR1B	0.09	2.08	1.99
<hr/>			
1019_C1	-	-	-
1019_C2*	0.95	-	-
1019_C3*	-	-	-
1019_C4	0.95	-	-
1019_C5*	-	-	-
1019_C6*	2.33	-	-
1019_C7	-	-	-
1019_C8*	-	-	-
1019_C9	0.95	-	-
1019_C10*	1.92	-	-
1019_CR1	-	-	-
1019_CR2^	0.87	-	-
1019_CR3	0.39	1.08	0.69
<hr/>			
1136_C1	-	-	-
1136_C2^	-	-	-
1136_C3*	-	-	-
1136_C4	-	-	-
1136_C5	1.14	-	-
1136_C6	0.81	-	-
1136_C7	0.10	1.61	1.52
1136_C8^	-	-	-
1136_C9	1.92	-	-
1136_C10*	-	-	-
1136_C11^	0.10	-	-
1136_C12	0.81	2.80	1.99
1136_CR1	0.81	-	-
1136_CR2	0.00	1.61	1.61
1136_CR3	0.00	1.61	1.61

Table 6 Initiation and Cracking Period - ECR (continued)

Specimen	Time to Initiation (yrs)	Time to Cracking (yrs)	Propagation time (yrs)
2021_C1	0.95	-	-
2021_C2*	1.36	-	-
2021_C3*	0.95	-	-
2021_C4^	-	-	-
2021_C5	0.87	-	-
2021_C6	0.09	1.04	0.96
2021_C7	0.55	-	-
2021_C8^	-	-	-
2021_C9*	0.55	-	-
2021_C10	-	-	-
2021_C11	0.87	-	-
2021_C12*	1.64	-	-
2021_CR1	0.55	1.04	0.50
2021_CR2^	-	-	-
2021_CR3*	-	-	-
2262_C1	1.05	-	-
2262_C2^	1.75	-	-
2262_C3	1.83	-	-
2262_C4	0.18	1.66	1.48
2262_C5	-	-	-
2262_C6	1.05	-	-
2262_C7^	0.80	-	-
2262_C8	0.18	1.66	1.48
2262_C9	1.38	-	-
2262_C10	0.47	1.66	1.19
2262_C11^	-	-	-
2262_C12	0.72	-	-
2262_CR1*	0.71	-	-
2262_CR2	0.10	1.91	1.81
2262_CR3*	2.67	-	-

Table 7 Initiation and Cracking Period - Bare Steel

Specimen	Time to Initiation (yrs)	Time to Cracking (yrs)	Propagation time (yrs)
6037_C1	0.08	0.67	0.58
6037_C2	0.08	0.67	0.58
6037_C3	0.17	1.45	1.28
6037_C5	0.08	1.72	1.64
6037_C7	0.46	1.43	0.96
6037_C8	0.08	0.67	0.58
6037_C9	0.79	1.70	0.91
6037_C10	0.46	2.83	2.37
6037_C11	0.08	0.73	0.64
6037_C12	0.47	1.90	1.43
6037_CR1/C4	0.08	1.72	1.64
6037_CR2/C6	0.08	1.43	1.34
<hr/>			
6128_C1	0.07	1.44	1.36
6128_C2	0.07	1.05	0.98
6128_C3	0.27	0.96	0.69
6128_C4	0.07	0.96	0.88
6128_C5	0.17	1.28	1.11
6128_C6	0.27	0.68	0.41
6128_C7	0.17	0.94	0.77
6128_C8	0.07	1.44	1.36
6128_C9	0.17	0.87	0.70
6128_C10	0.17	0.94	0.77
6128_C11	0.63	0.87	0.24
6128_C12	0.08	1.44	1.36
6128_CR1	0.07	0.87	0.80
6128_CR2	0.07	0.68	0.61
6128_CR3	0.08	1.00	0.92
6128_CR4	0.08	1.44	1.36

Additional Testing for ECR Specimens

Description of ECR Specimen Selection Process for Additional Testing

A total of 54 ECR specimens were selected for further testing in the present study. The 54 specimens that were selected are outlined in Table 8. The selected specimens from the previous phase of the study include 6 that had been truncated and 16 that had cracked. In addition, 30 specimens were selected from the present phase of the study and 2 that had cracked.

Table 8 Summary of ECR Specimens Selected for Further Testing

Truncated specimens from previous study	6
Cracked specimens from previous study	16
Truncated during present study	30
Cracked during present study	2
Total	54

The 54 specimen set includes a 22 specimen subset that either cracked or truncated during the time that the previous study was conducted. Approximately 3 specimens were selected to represent each of the ECR bridges, with the exception of the 1001 and 2262 bridges, which had 1 and 4 specimens, respectively. One truncated specimen was selected to represent each bridge, where applicable. Table 9 presents the age, time to corrosion initiation, time of corrosion propagation (where applicable), and shelf life. The shelf life measures the time the epoxy specimens were stored in plastic bags after Brown's evaluation until testing during the present study. The time of corrosion propagation is a measurement of time between corrosion initiation and the time of cracking.

Table 9 ECR Samples Selected for Testing from Previous Study

^ Specimens truncated prior to cracking from previous study

Bridge (name)	Sample (#)	Age (yrs)	Initiation (yrs)	Propagation (yrs)	Shelf Life (yrs)
1136	C7	4	0.10	1.52	0.89
1136	C11^	4	0.10	-	0.67
1136	CR3	4	0.00	1.61	0.84
1004_6	C3^	6	-	-	0.67
1004_6	C7	6	0.09	1.78	0.61
1004_6	C11	6	0.55	0.48	1.46
1001	C2	7	0.90	0.99	0.61
1019	CR2^	9	0.87	-	0.67
1019	CR3	9	0.39	0.69	0.89
1015	C1	12	1.18	0.67	0.65
1015	C10	12	0.09	1.85	0.56
1015	CR3	12	0.09	1.76	0.65
2262	C8	14	0.18	1.48	0.84
2262	C10	14	0.47	1.19	0.65
2262	C11^	14	-	-	0.67
2262	CR2	14	0.10	1.81	0.59
1004_3	C1	16	0.18	1.75	0.57
1004_3	C3	16	0.81	1.12	0.57
1004_3	C9^	16	0.57	-	0.67
2021	C4^	18	-	-	0.67
2021	C6	18	0.09	0.96	1.46
2021	CR1	18	0.55	0.50	1.42

In addition, 30 specimens were selected from the remaining uncracked ECR cores to be truncated and undergo further testing in the present study. The core selection process considered 15 cores that had experienced corrosion initiation and 15 that had not. These samples were selected at random and did not take the bridge identification into account. As a result, the number of samples that represent each bridge varies. The samples selected for truncation and testing are presented in Table 10, which includes the age and time to corrosion initiation (where applicable). This data set does not include a propagation or shelf life time as they do not apply. All testing for this set was conducted at the approximate time the core was autopsied.

Table 10 ECR Samples Selected for Truncation and Testing from Present Study

Bridge (name)	Sample (#)	Age (yrs)	Initiation (yrs)
1136	C3	4	-
1136	C10	4	-
1004_6	C4	6	-
1004_6	C10	6	-
1001	C3	7	-
1001	C5	7	-
1001	C6	7	-
1001	C7	7	-
1001	CR3	7	-
1019	C3	9	-
1019	C5	9	-
1019	C8	9	-
1004_3	C6	16	-
1004_3	C7	16	-
2021	CR3	18	-
1004_6	C5	6	2.58
1019	C2	9	0.95
1019	C6	9	2.33
1019	C10	9	1.92
1015	C2	12	1.18
1015	C5	12	0.57
1015	C7	12	0.1
2262	CR1	14	0.71
2262	CR3	14	2.67
1004_3	C2	16	0.38
1004_3	C11	16	0.18
2021	C3	18	0.95
2021	C9	18	0.55
2021	C12	18	1.64
2021	C2	18	1.36

The remaining 2 cores included in the present study are specimens that had cracked as a result of corrosion. The specimens are listed in Table 11, which includes information on the age, time to corrosion initiation, propagation time, and time to cracking.

Table 11 Cracked Samples Selected from Present Study

Bridge (name)	Sample (#)	Age (yrs)	Initiation (yrs)	Propagation (yrs)	Cracking (yrs)
1136	C12	4	0.81	1.99	2.80
1015	C6	12	0.09	2.95	3.04

Test Results Summary

Tests were conducted to evaluate the epoxy coating moisture content, glass transition temperatures (T_g), and the epoxy coating crack frequency for selected ECR samples. The epoxy moisture content was measured for all 54 specimens while the initial T_g , fully-cured T_g , and crack frequency values are only presented for the 22 specimens from the previous study. The test results for the previous and present study specimens are presented in Tables 12 and 13, respectively. Test results for the coating thickness, holidays, and adhesion were obtained for all 54 of the specimens from Pyc's study (Pyc, 1998). The percent saturation for the voids in the concrete after ponding was limited to testing conducted in the present study and is presented in Table 14.

Glass Transition Temperatures

The glass transition temperature (T_g) was measured for all 22 specimens from the previous study and the results ranged from 64.54°C to 102.64°C, as shown in Table 12.

All specimens that were tested for the T_g were also evaluated to determine fully-cured T_g measurements. Epoxy samples, measuring 4.0g, were selected for each ECR specimen to be completely polymerized through additional heat treatment. The description for this procedure is outlined in the Methods and Materials section. Subsequent to the polymerization procedure, the fully-cured T_g measurements were taken and the results for all specimens ranged between 97.45°C and 116.54°C. These results are presented in Table 12.

The difference in temperature between its T_g value and its fully-cured T_g potential were noted and greater differences in the T_g values indicated the coatings were less developed. The plot in Figure 5 shows the initial T_g value and the fully-cured T_g potential values for the 22 specimens from the previous phase of study. As you can see, the difference in temperatures reveals that none of these samples tested in this study have reached its fully cured potential.

Table 12 ECR Data Summary for % Epoxy Moisture, Glass Transition Temperatures, and Crack Frequency

Classification	Bridge #	Age (yrs)	Initiation (yrs)	Propagation (yrs)	Epoxy Moisture (%)	Tg (°C)	Full Tg (°C)	Δ Tg (°C)	Cracking (#)	
Samples from previous study (* truncated samples)	1136	C7	4	0.10	1.52	1.05	82.12	103.62	21.50	1
	1136	C11*	4	0.10	-	0.39	93.99	104.09	10.10	1
	1136	CR3	4	0.00	1.61	0.48	91.34	102.05	10.71	1
	1004_6	C3*	6	-	-	1.14	83.85	116.54	32.69	4
	1004_6	C7	6	0.09	1.78	0.60	82.27	112.36	30.09	3
	1004_6	C11	6	0.55	0.48	0.42	84.85	112.92	28.07	2
	1001	C2	7	0.90	0.99	0.50	102.64	112.86	10.22	1
	1019	CR2*	9	0.87	-	0.84	89.17	113.25	24.08	2
	1019	CR3	9	0.39	0.69	0.68	85.23	114.55	29.32	3
	1015	C1	12	1.18	0.67	0.92	81.95	113.67	31.72	2
	1015	C10	12	0.09	1.85	0.81	87.85	115.14	27.29	2
	1015	CR3	12	0.09	1.76	1.39	70.39	114.39	44.00	1
	2262	C8	14	0.18	1.48	1.03	66.80	115.73	48.93	4
	2262	C10	14	0.47	1.19	0.91	68.09	115.36	47.27	4
	2262	C11*	14	-	-	0.92	64.54	114.55	50.01	3
	2262	CR2	14	0.10	1.81	1.17	86.23	112.93	26.70	3
	1004_3	C1	16	0.18	1.75	0.33	69.45	107.86	38.41	2
	1004_3	C3	16	0.81	1.12	1.27	86.35	105.98	19.63	1
	1004_3	C9*	16	0.57	-	1.10	85.84	107.25	21.41	1
	2021	C4*	18	-	-	0.61	84.39	97.45	13.06	1
	2021	C6	18	0.09	0.96	0.61	85.04	90.90	5.86	2
	2021	CR1	18	0.55	0.5	0.57	84.83	102.67	17.84	1

Figure 5 The initial T_g value and the fully-cured T_g potential values for the 22 specimens from the previous phase of study

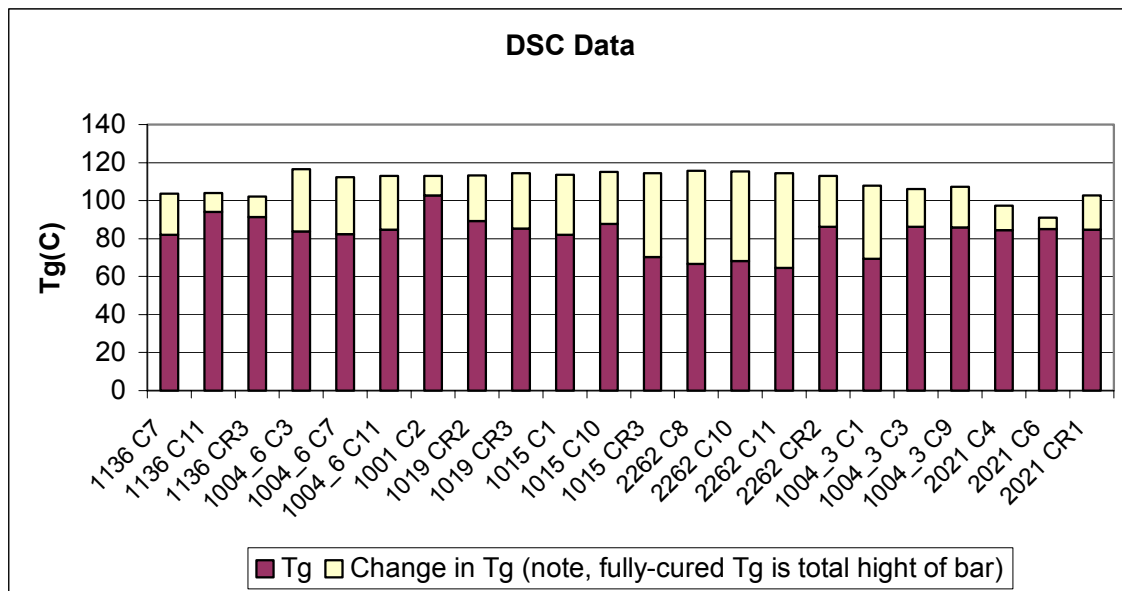


Table 13 ECR Data Summary for % Epoxy Moisture from Present Study

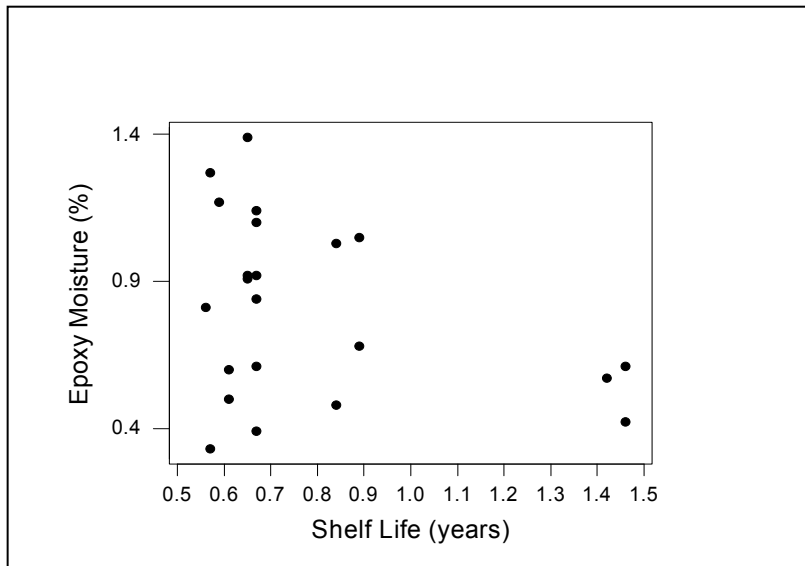
Classification	Bridge #	Age (yrs)	Initiation (yrs)	Propagation (yrs)	Epoxy Moisture (%)	
Truncated samples from present study	1136	C3	4	-	-	1.06
	1136	C10	4	-	-	0.82
	1004_6	C4	6	-	-	2.10
	1004_6	C10	6	-	-	1.22
	1001	C3	7	-	-	1.01
	1001	C5	7	-	-	1.13
	1001	C6	7	-	-	1.07
	1001	C7	7	-	-	0.89
	1001	CR3	7	-	-	1.02
	1019	C3	9	-	-	1.05
	1019	C5	9	-	-	0.97
	1019	C8	9	-	-	1.12
	1004_3	C6	16	-	-	0.83
	1004_3	C7	16	-	-	0.33
	2021	CR3	18	-	-	0.41
	1004_6	C5	6	2.58	-	1.24
	1019	C2	9	0.95	-	1.09
	1019	C6	9	2.33	-	1.17
	1019	C10	9	1.92	-	1.17
	1015	C2	12	1.18	-	0.88
	1015	C5	12	0.57	-	1.09
	1015	C7	12	0.10	-	0.59
	2262	CR1	14	0.71	-	1.15
	2262	CR3	14	2.67	-	0.98
	1004_3	C2	16	0.38	-	1.24
	1004_3	C11	16	0.18	-	0.97
	2021	C2	18	1.36	-	1.21
	2021	C3	18	0.95	-	0.99
	2021	C9	18	0.55	-	1.56
	2021	C12	18	1.64	-	1.06
Cracked	1136	C12	4	0.81	2.75	0.48
	1015	C6	12	0.09	2.95	1.10

Moisture Content of Epoxy Coating

The moisture content of the coating was measured by weight for all 54 ECR specimens and ranged between 0.33% and 2.10%. The values obtained from specimens of the previous study ranged from 0.33% to 1.39% and averaged 0.81%. Truncated and cracked specimens from the present study ranged from 0.33% to 2.10% and averaged 0.99%. These values are shown in Tables 12 and 13.

The relationship between the shelf life (defined earlier as the storage time for the ECR after specimen autopsy) for a sample and the percent epoxy moisture content was investigated to determine if the shelf life would lead to moisture loss of the sample over time. The shelf life was only applicable to specimens from the previous phase of the study and their storage time ranged between 0.56 years and 1.46 years. The results for the correlation, plotted in Figure 6, indicate that there is no significant relationship. Regardless of the shelf life of any given sample, the moisture content was typically just under 1%. As a result, the shelf life appeared to have an unbiased effect on the percent epoxy moisture and these values could be incorporated into further analysis of this study.

Figure 6 Shelf Life versus % Epoxy Moisture Content



Crack Frequency

The crack frequency within the coating surface was estimated for the 22 specimens selected from the previous study. Figure 7 presents typical rating results for SEM photographs with a 2K magnification and the results are presented in Table 12.

Holidays

The number of holidays was measured for each specimen through use of a holiday detector in the previous study made by Pyc (Pyc, 1998). The average number of holidays for each specimen from the study ranged between 0 and 4 with the exception that a specimen from bridge 1001 had 7 holidays and a specimen from bridge 1015 had 10 holidays. Information on holidays is included in Table 14

Table 14 ECR Data Summary for Epoxy Coating Thickness, Holidays, & Adhesion; Concrete Saturation

Classification	Bridge #	Age (yrs)	Initiation (yrs)	Prop. (yrs)	Thickness (μm)	Holiday (#)	Adhesion (#)	Concrete Saturation (%)	Void Saturation (%)
Truncated Samples from present study	No corrosion initiation	1136 C3	4	-	-	244	1	1	75.04
		1136 C10	4	-	-	172	0	1	86.07
		1004_6 C4	6	-	-	256	0	3	90.29
		1004_6 C10	6	-	-	238	0	5	86.89
		1001 C3	7	-	-	304	2	2	77.31
		1001 C5	7	-	-	236	2	5	80.61
		1001 C6	7	-	-	209	3	2	91.39
		1001 C7	7	-	-	209	1	1	73.06
		1001 CR3	7	-	-	-	-	-	98.96
		1019 C3	9	-	-	138	0	5	98.96
		1019 C5	9	-	-	169	0	4	74.42
		1019 C8	9	-	-	168	0	5	92.38
		1004_3 C6	16	-	-	253	2	1	98.13
		1004_3 C7	16	-	-	192	3	1	76.73
		Initiated Corrosion	2021 CR3	18	-	-	310	-	-
	1004_6 C5		6	2.58	-	303	0	5	89.05
	1019 C2		9	0.95	-	146	0	5	96.79
	1019 C6		9	2.33	-	172	0	4	89.15
	1019 C10		9	1.92	-	-	-	-	85.68
	1015 C2		12	1.18	-	215	0	2	98.90
	1015 C5		12	0.57	-	154	3	5	99.36
	1015 C7		12	0.10	-	257	3	1	92.27
	2262 CR1		14	0.71	-	210	-	-	94.36
	2262 CR3		14	2.67	-	120	-	-	96.09
	1004_3 C2		16	0.38	-	154	4	2	98.98
	1004_3 C11		16	0.18	-	163	2	1	96.06
	2021 C2	18	1.36	-	192	1	5	66.89	
2021 C3	18	0.95	-	273	2	1	74.90		
2021 C9	18	0.55	-	223	2	5	93.70		
2021 C12	18	1.64	-	197	3	4	92.97		
Cracked, present study	1015 C6	12	0.09	2.95	152	10	5	87.97	
1136 C12	4	0.81	1.99	185	3	1	-		
Samples selected from previous study (* truncated samples)	1136 C7	4	0.10	1.52	301	0	1	-	
	1136 C11*	4	0.10	-	231	0	1	-	
	1004_6 C3*	6	-	-	263	0	2	-	
	1004_6 C7	6	0.09	1.78	229	2	5	-	
	1004_6 C11	6	0.55	0.48	286	0	1	-	
	1001 C2	7	0.90	0.99	219	7	5	-	
	1015 C1	12	1.18	0.67	339	2	5	-	
	1015 C10	12	0.09	1.85	227	0	1	-	
	2262 C8	14	0.18	1.48	90	0	4	-	
	2262 C10	14	0.47	1.19	160	1	1	-	
	2262 C11*	14	-	-	220	0	1	-	
	1004_3 C1	16	0.18	1.75	167	2	2	-	
	1004_3 C3	16	0.81	1.12	170	2	1	-	
	1004_3 C9*	16	0.00	0.57	189	0	1	-	
	2021 C4*	18	-	-	202	2	3	-	
2021 C6	18	0.09	0.96	238	1	1	-		

Thickness

The coating thickness was measured at 12 locations for each ECR specimen, with 6 readings on both the top and bottom sections, and an average value for each specimen was obtained. Average thickness ranged from 90μm to 339μm for the entire 54 ECR specimen set and results are located in Table 14.

Adhesion

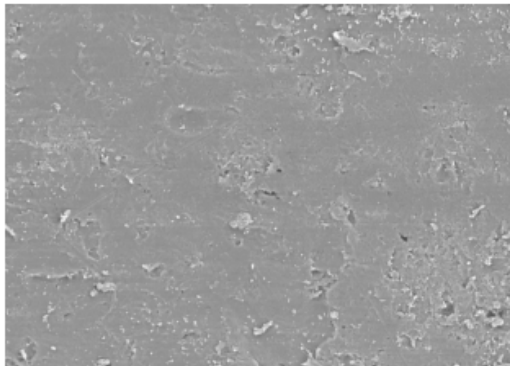
The adhesion rating was determined using a knife-peel test described in the Methods & Materials section. Values ranged between 1 and 5, with 1 representing excellent adhesion and 5 indicating poor adhesion. The adhesion results are listed in Table 14.

Percent Saturation of Voids in Concrete at Bar Depth

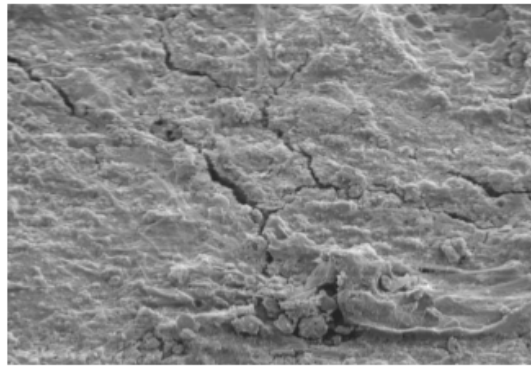
The percent saturation in the voids for the concrete encasing the ECR was measured for the 30 truncated cores from the present study. The results ranged between 73.06% and 99.36%, with an average at 66.89%. The percent saturation data are provided in Table 14.

Figure 7 Typical Rating Results for epoxy Surface Cracks from SEM Photographs with a 2K Magnification Measured on a scale of 1 to 4 (where 1 has no surface cracks and 4 is severely cracked)

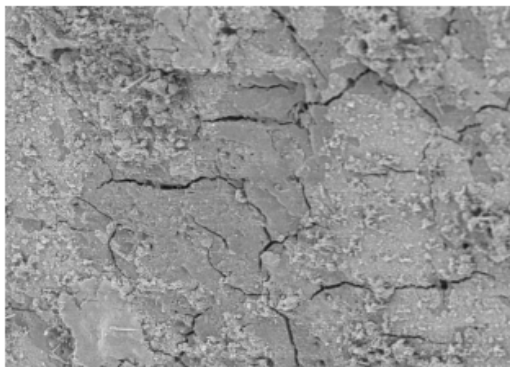
10µm

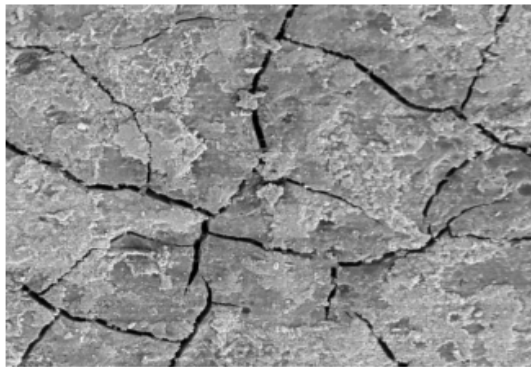
1



2



3



4

ANALYSIS AND DISCUSSION

The analysis and discussion in this chapter is divided into three sections. The first section examines the updated results from all testing continued from the previous study. The previous phase of this study monitored the specimens for approximately 1.94 years while the current study continued monitoring for an additional 1.12 years. The information in this section considers all data collected for the entire 3.06 year testing period and includes observations of specimens for corrosion initiation, corrosion-induced cracking, and assessing the chloride levels for the concrete adjacent to the reinforcing steel. The second section focuses on testing procedures that were unique to the current study with an emphasis on epoxy coating parameters. The epoxy parameters that are discussed in this section include the glass transition temperature (T_g), the percent moisture content, cracking frequencies, and the crack widths. Finally, this last section takes all concrete and epoxy parameters into account and examines the relationships to corrosion initiation time and cracking time.

Section One: Continued Testing for Laboratory Core Evaluations

All 141 samples underwent laboratory treatment and measurements were made on their time to initiation, time to cracking, and chloride content for both ECR and bare steel reinforcement where applicable. The results in this section were used to examine the advantages of using ECR in comparison to bare steel reinforcement.

Table 15 presents a summary of the average time periods for both chloride-induced corrosion initiation and corrosion-induced cracking to occur. The propagation time is also included in the table and represents the calculated time from corrosion initiation to the time of cracking. The table shows that the average propagation period is not equal to the difference in averages between the time to initiation and the time to cracking for ECR because many of the ECR specimens that have initiated corrosion have not experienced cracking. The average propagation period for ECR in Table 15 represents the 25 ECR specimens that have undergone both corrosion initiation and corrosion-induced cracking.

Table 15 Summary of Average Time Periods for Chloride-Induced Corrosion Initiation, Corrosion-Induced Cracking, and Propagation for Bare Steel and ECR

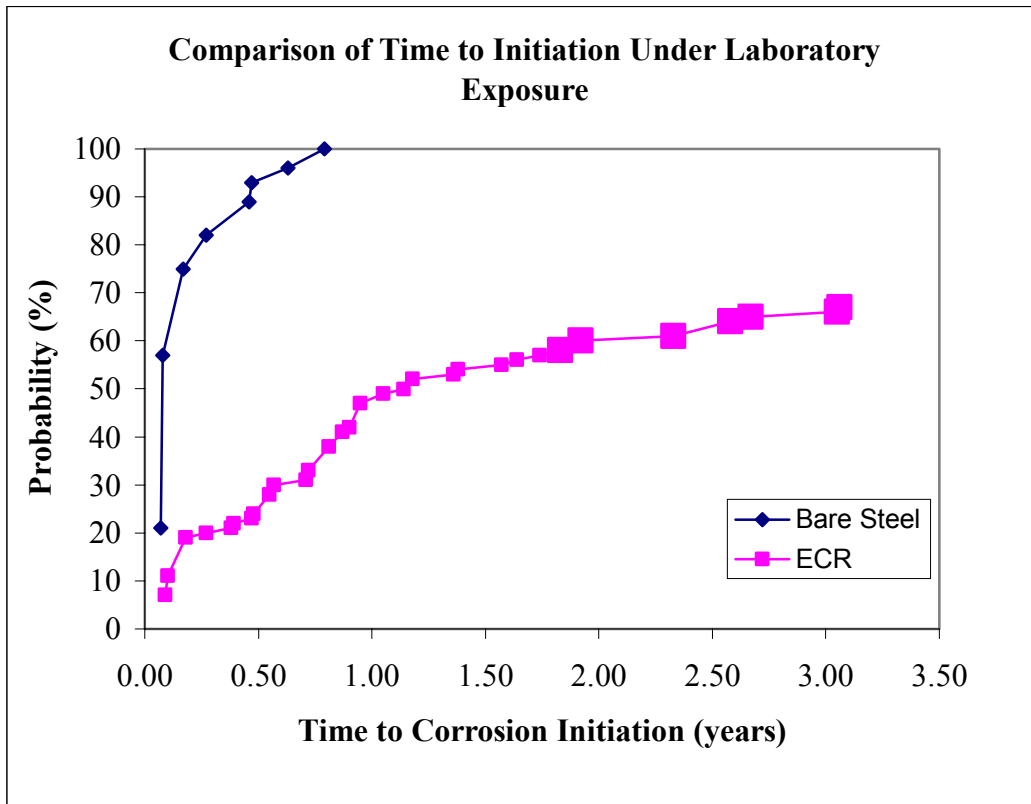
		Time to Initiation (years)	Time to Cracking (years)	Propagation Period (years)
Bare Steel	Average	0.20	1.21	1.01
	StDev	0.19	0.49	0.46
	CoV	95%	40%	46%
	N	28	28	28
ECR	Average	0.88	1.75	1.42
	StDev	0.78	0.49	0.57
	CoV	89%	28%	40%
	N	64	25	25

Also in Table 15, the time to initiation and the time to cracking were evaluated for all 28 bare steel specimens. Although there were a total of 113 ECR specimens that were tested during this study, results for the 17 truncated specimens from the previous phase were not considered in Table 15, as well as Figures 8,9, and 10. These 17 specimens could not be compared with the other ECR because they were truncated after approximately 1.67 years and, consequently, information for their time to initiation and corrosion-induced cracking is incomplete. However, data on the 30 specimens that were truncated during the current phase of the study were applicable at the time of autopsy because they had an opportunity to experience corrosion monitoring for the complete testing period, approximately 3.06 years. Collectively, the ECR data is based on the remaining 96 specimens, where 64 initiated corrosion and 25 cracked by the end of the laboratory treatment.

Time to Corrosion Initiation

Figure 8 demonstrates the corrosion initiation rate by plotting the initiation probability as a function of time. All bare steel samples underwent corrosion initiation while 67% of the ECR reached corrosion initiation during the 3.06 year ponding treatment period.

Figure 8 Corrosion Initiation Rate for Bare Steel and ECR Specimens
Note: Larger data points represent data updated during the current study, from 1.94 years to 3.06 years



All the bare steel specimens reached corrosion initiation within 0.79 years of ponding treatment application with more than half of the specimens initiated corrosion within 0.17 years. The probability for ECR specimens to reach corrosion initiation steadily increased to over 50% during the first 1.5 years of ponding treatment. Subsequently, the rate for ECR probability to initiate corrosion declined considerably.

Figure 8 indicates that the probability for corrosion initiation developed steadily within the first 1.5 years of ponding treatment. The trend for the decline after 1.5 years indicates there were a percentage of cores that were able to successfully protect the reinforcing steel throughout the 3.06 year ponding treatment. Furthermore, the decline in the corrosion initiation rate indicates that it is becoming more likely for this group to withstand corrosion initiation over time. When considering this occurrence, ECR might be classified in two distinct groups; those that are likely to initiate corrosion early, and those that are not. The graph illustrates that more than half of the ECR specimens tested were classified in a group that was not successful in providing corrosion protection.

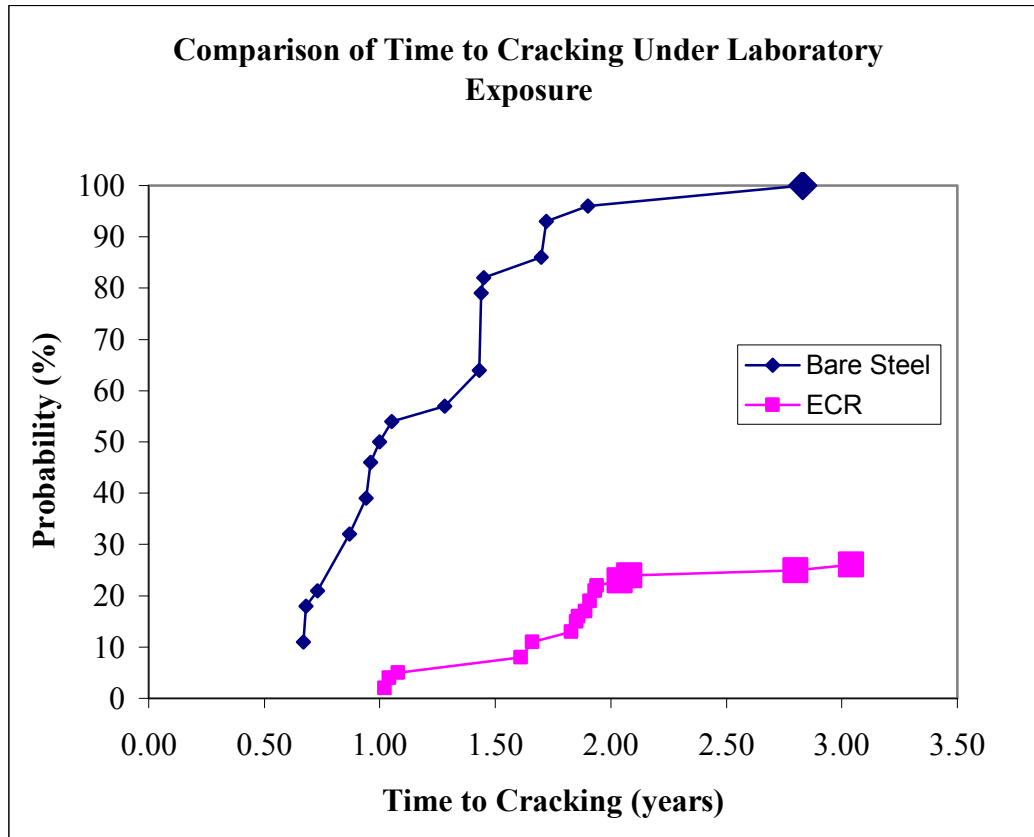
Time to Corrosion-Induced Cracking

In Figure 9, the graph for the rate of corrosion-induced cracking shows that the bare steel specimens began to crack at 0.67 years while the first ECR sample cracked at 1.02 years. The rate of ECR started out very slowly but underwent a rapid increase between 1.7 and 1.9 years, followed by a decline during the remainder of the testing period. All bare steel samples have cracked to date and the probability of cracking appeared to develop at a fairly uniform rate.

The decline in probability for corrosion-induced cracking to occur for ECR supports the decline in corrosion initiation, where both probabilities wane as the ponding treatment duration reached 2.0 years. The argument that the specimens may be classified into two groups can also be applied to their likelihood of cracking.

Comparison of the time to initiation (Figure 8) and the time to cracking (Figure 9) reveals that many of the ECR specimens that initiated corrosion did not undergo cracking within the study period. As a result, two separate groups can be further identified from the ECR specimens that have initiated corrosion; those that corroded severely enough to lead to surface cracks and those that have not. Although the overall cracking probability at the end of the 3.06 year ponding treatment is 26% for ECR while 100% probability for bare steel, there is indication that the damage for the ECR is still substantial enough to question its overall performance in field applications. For example, it has been stated that a structure will require rehabilitation once 12% of the pavement surface of the worst span lane has been damaged (Fitch, M. G. et al., 1995). Furthermore, noting the time that it takes for cracking damage to take place in Figure 6 shows an extension of nearly one year for ECR when compared to bare steel. These laboratory results were used in the previous phase for this study to estimate the service life extension to be approximately 5 years when substituting ECR for bare steel in field structures (Brown, 2002).

Figure 9 Corrosion-Induced Cracking Rate for Bare Steel and ECR Specimens
Note: Larger data points represent data updated during the current study, from 1.94 years to 3.06 years

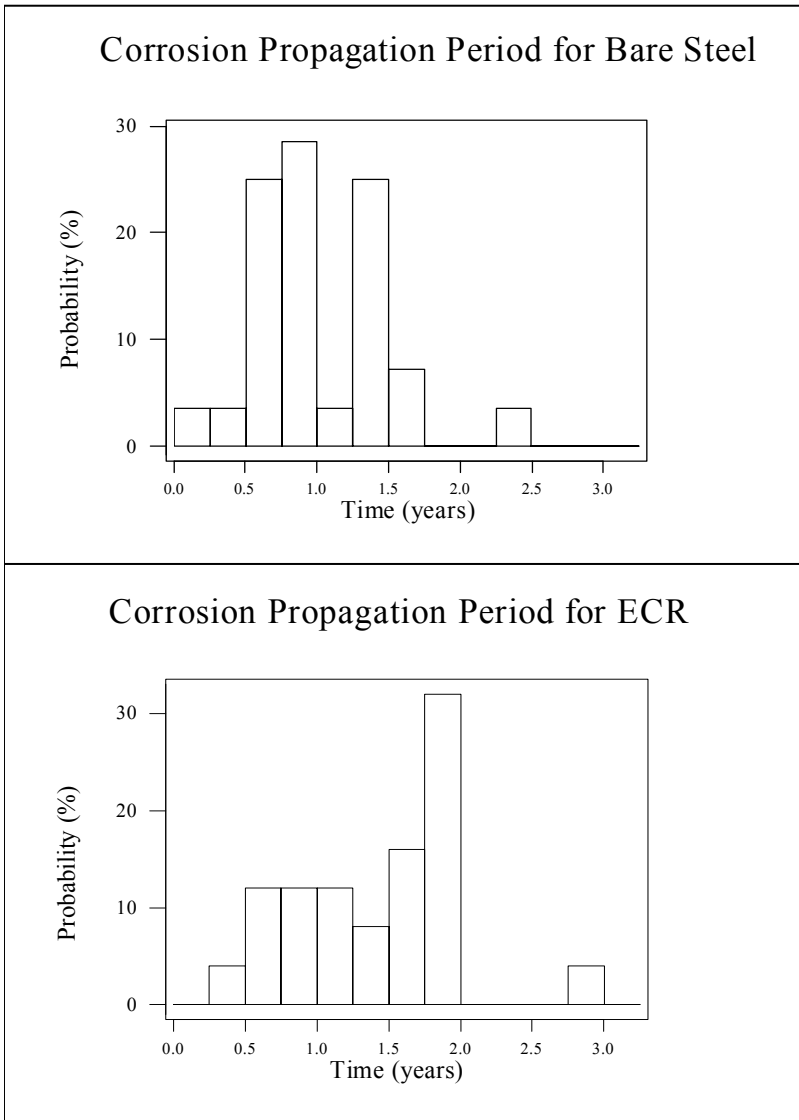


Propagation Time

Figure 10 provides histograms for the propagation time for both bare steel and ECR. The propagation time measures the amount of time that takes place from corrosion initiation to the time of cracking. The bare steel specimens had an average propagation time of 1.01 years and ranged between 0.24 years and 2.37 years. The ECR specimens averaged 1.42 years and ranged between 0.48 years and 2.95 years. Normality tests were conducted for the propagation time data and both bare steel and ECR data sets were consistent with a normal distribution trend.

It can be seen that the average propagation period for ECR is extended by 0.41 years in comparison to bare steel. This result is comparable to the previous study that yielded an average propagation time extension period of 0.33 years.

Figure 10 Histograms of Corrosion Propagation Period for Bare Steel and ECR



Min: 0.24
 1st Qu: 0.65
 Mean: 1.01
 Median: 0.92
 3rd Qu: 1.36
 Max: 2.37
 Total N: 28
 StDev: 0.46

Min: 0.48
 1st Qu: 0.98
 Mean: 1.42
 Median: 1.52
 3rd Qu: 1.80
 Max: 1.37
 Total N: 25
 StDev: 0.57

Chloride at Bar Depth at Cracking

Chloride concentration values at bar depth were measured for each specimen at the end of their ponding treatment. These values were used to estimate the chloride concentration at bar depth at the time of corrosion initiation.

A total of 30 ECR specimens were selected to be truncated upon completion of the 3.06 year study. The chloride contents at the reinforcement depth for the truncated specimens were compared to those of the cracked specimens using histograms that are presented in Figure 11. A two sample t-test revealed that the two populations were significantly different, with a p-value of 0.01, and, as a result, the chloride concentrations for these 30

truncated specimens were not classified with the cracked specimens in further analysis. The chloride concentration was determined using a 2,323 kg/m³ nominal concrete density and the diffused chloride was calculated by deducting the nominal background chloride concentration for every bridge structure.

Figure 11 Comparison of Chloride Concentration (kg/m³) at Bar Depth: Cracked versus Truncated ECR Specimens

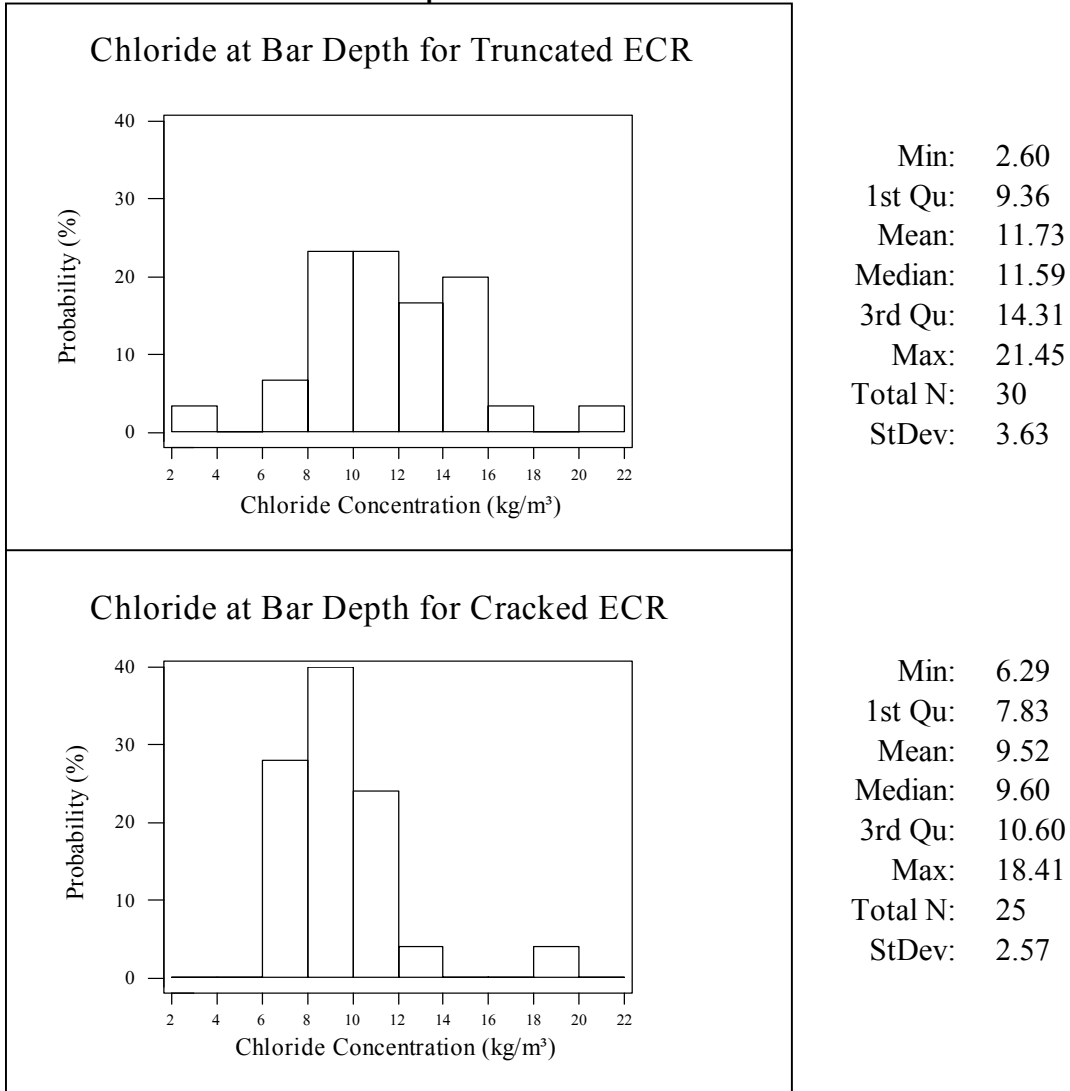
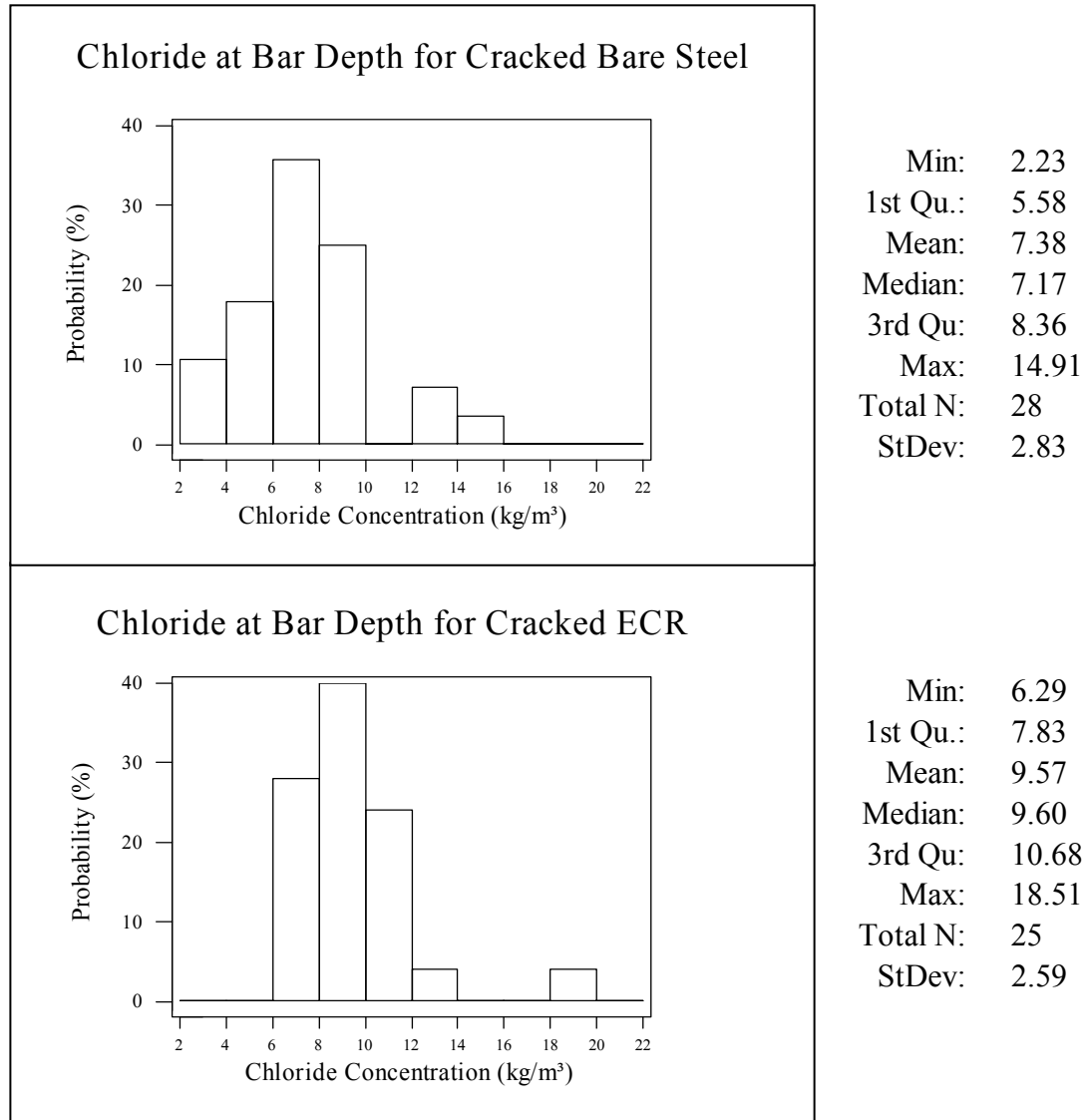


Figure 12 presents the chloride content histograms at cracking for both bare steel and ECR. The average chloride concentration for bare steel was 7.38 kg/m³ and the values ranged between 2.23 kg/m³ and 14.91 kg/m³. The ECR chloride concentration averaged 9.57 kg/m³ and the values ranged between 6.29 kg/m³ and 18.51 kg/m³. Collectively, the ECR specimens exhibited a tendency for possessing higher chloride concentrations at the time of cracking. These results are similar to the previous study which yielded an average of 7.10 kg/m³ and 9.41 kg/m³ for bar steel and ECR specimens, respectively.

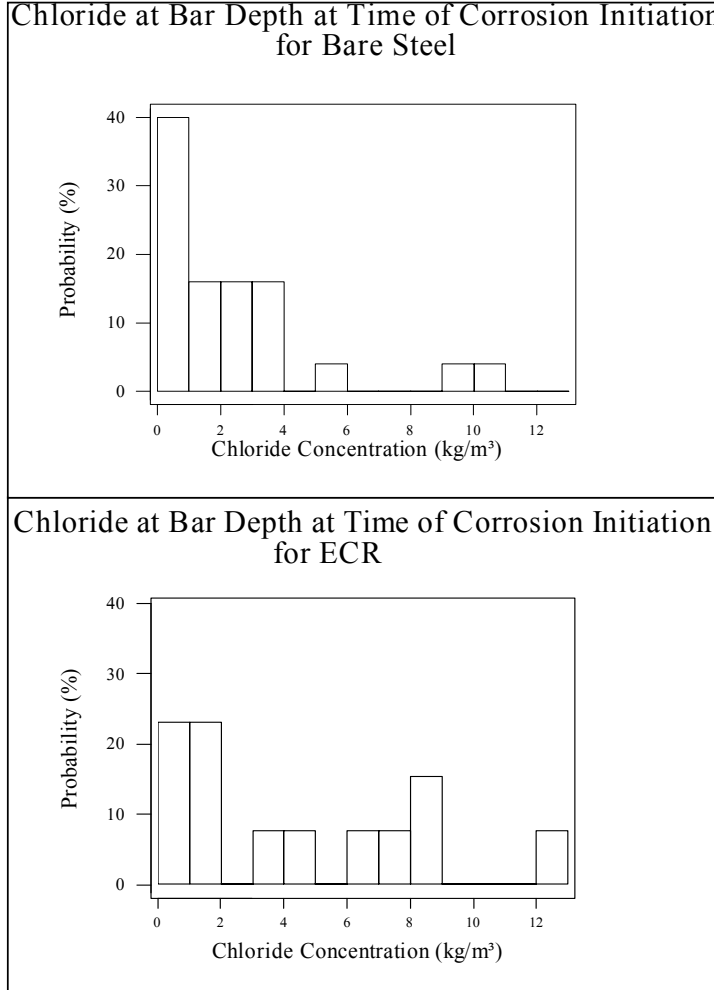
Figure 12 Chloride Concentration (kg/m³) at Bar Depth at Cracking: for Bare Steel and ECR



Estimating Chloride at Bar Depth at Initiation

The effective diffusion rates for chlorides were investigated before laboratory treatment. In addition, the diffusion rate was also calculated once the core completed ponding treatment. Throughout the duration of the ponding treatment, cores became increasingly saturated. As a result, the chlorides were expected to migrate in a diffusion-controlled fashion and the diffusion equation, Fick's 2nd law, was applied to assess the diffusion rate for all applicable specimens. The diffusion rate was determined using Equation 1 by noting the chloride values directly above and adjacent to the bar at the end of ponding

Figure 13 Estimate of Chloride Concentration (kg/m³) at Bar Depth at Corrosion Initiation for ECR and Bare Steel (BS)



Min: 0.01
 1st Qu: 0.41
 Mean: 2.4
 Median: 1.55
 3rd Qu: 3.27
 Max: 10.00
 Total N: 25
 StDev: 2.64

Min: 0.08
 1st Qu: 0.98
 Mean: 4.42
 Median: 3.59
 3rd Qu: 7.81
 Max: 12.68
 Total N: 13
 StDev: 3.89

treatment. Once the diffusion rate was calculated, it was reapplied to the diffusion equation to estimate the amount of chloride that existed at bar depth at the time of corrosion initiation.

The diffusion coefficients that were estimated after laboratory treatment were, typically, an order of magnitude greater than estimates made prior to treatment, which were based upon in-service chloride exposure. This is to be expected due to the increase of pore-water saturation in the concrete throughout the duration of the ponding treatment. Because corrosion initiation typically occurred during the accelerated laboratory treatment, it is appropriate to use the diffusion coefficients that were calculated *after* laboratory treatment when estimating the chloride concentration at bar depth at the time of corrosion-induced initiation.

The histograms for the estimated values of chloride at the time of corrosion initiation are presented in Figure 13 and compares values for the applicable specimens, which totaled 25 for bare steel and 13 for ECR. The amount of chloride estimated at corrosion

initiation for bare steel averaged 2.40 kg/m³ and ranged between 0.01 kg/m³ and 10.00 kg/m³. The average amount of chloride at corrosion initiation that was estimated for cracked ECR specimens is at 4.42 kg/m³ and ranged between 0.08 kg/m³ and 12.68 kg/m³. The chloride concentration distribution for ECR was tested for normality and was consistent with a normal trend.

A two sample t-test was applied to the bare steel and ECR samples for the level of chloride at the time of initiation. The results, with p-value of 0.11, indicated that there was no significant difference in the estimated level of chloride initiation concentrations. Although the ECR specimens have a higher chloride concentration average than bare steel, the two populations are comparable when applied to the two sample t-test because ECR has a much higher variance. Many of the ECR chloride concentrations at initiation are similar to those of bare steel.

The above results corroborate the results from the previous study, which determined there was effectively no difference in the chloride concentrations at the time of corrosion-induced initiation between bare steel specimens and ECR specimens that have experienced early deterioration (Brown, 2002). It is important to note that the estimated chloride concentrations at the time of corrosion initiation are from ECR specimens that underwent corrosion that was severe enough to lead to surface cracks. In addition, the majority of specimens from this population have cracked within the first 2.00 years of the NaCl ponding application process.

Summary and Significance for the Updated Results

Initially, one may interpret by these data that ECR effectively enhances bridge deck performance when used instead of bare steel. Results that favored ECR performance to bare steel were acknowledged by lower probability for corrosion initiation, lower probability for time to corrosion-induced cracking, extended propagation periods, and lower chloride concentration at bar depth for all cracked specimens. Despite these trends, it is important to emphasize that these data can be misleading and to surmise ECR is providing adequate corrosion prevention would be inaccurate. Regardless of the effects ECR may have on preventing corrosion in the short term, the long term performance for extending the service life of bridge decks must also be taken into account. The previous study approximated that ECR would extend the service life of highway bridge decks by 5 years and determined this was not cost-effective (Brown, 2002).

Collectively, the present study exhibited trends in the data that corroborated with the previous study. They both acknowledge that there are some improvements in performance when considering the extended propagation periods and the increase in chloride concentrations at the time to cracking. But the updated results also support the previous findings showing these improvements for ECR are not substantial and that there continues to be no significant difference between chloride concentrations levels between ECR and bare steel at the time of corrosion initiation.

Section Two: Testing of the Epoxy Coating

Initial T_g

The glass transition temperature (T_g) was measured for each epoxy sample of a 22 sample subset for specimens that had either cracked or had been truncated during the previous phase of this study. The average T_g value measured was 82.60°C and the values ranged between 64.54°C and 102.64°C. The histogram for the T_g is presented in Figure 14.

The literature explains that the T_g for a given sample is determined by its chemical structure (Stevens, M. P., 1999). The thermogram results for the DSC tests demonstrated conclusively that the epoxy networks were not fully-cured at the time of manufacture by revealing a curing exotherm at temperatures above the T_g . Furthermore, the variance for the initial T_g values indicates that the chemical structure of the epoxy coating is highly inconsistent upon completion of the coating application process. Other factors related to aging may have further altered the chemical composition for the epoxy coating by causing the T_g to increase over time. For example, if the epoxy network is exposed to ultraviolet light during the construction process, additional curing can take place that will cause the T_g to elevate. Also, the presence of moisture may also increase the T_g over time as water molecules chemically react with the epoxy network. Although these changes in T_g may occur over time, it is important to note that their overall effect on altering initial T_g for the epoxy network will only be a few degrees Celsius, if at all.

The extent that water will increase the T_g can be directly calculated with the following equation (Cowie, 1991):

$$1/T_g = w_1/T_{g1} + w_2/T_{g2} \quad \text{Equation 2}$$

where,

T_g = the T_g of the sample that has been exposed to moisture, measured by DSC

w_1 = percentage of water weight in the epoxy network, measured by TGA

T_{g1} = T_g of water, approximately -137.15°C

w_2 = percent weight for the epoxy network that does not include moisture, 100% – w_1

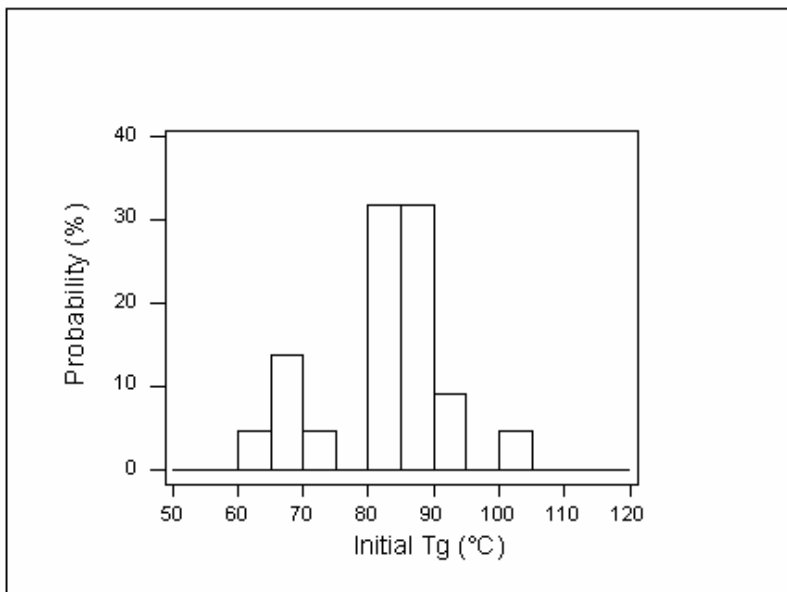
T_{g2} = the T_g of the network before exposure to moisture

An example for measuring the T_g of the network before exposure to moisture is provided and demonstrates the negligible effects that moisture will have on the T_g . The data for this example uses the average values measured from the 22 sample set, yielding a T_g at 82.60°C and the w_1 at 0.81%. When these data are applied to Equation 2, it yields

$$1/82.60^\circ\text{C} = 0.81\% / (-137.15^\circ\text{C}) + 99.19\% / T_{g2}$$

Solving this equation results with $T_{g2} = 81.53^\circ\text{C}$ and, in effect, approximates that the water altered the T_g by increasing it by 1.07°C.

Figure 14 Histogram of Initial T_g Values (C°)

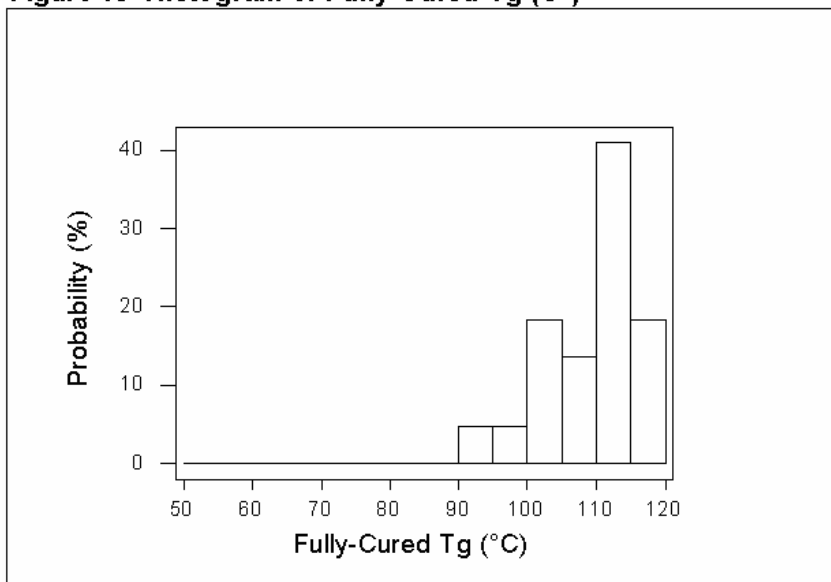


Min:	64.54
1st Qu.:	79.06
Mean:	82.60
Median:	84.84
3rd Qu.:	86.72
Max:	102.64
Total N:	22
StDev:	9.39

Fully-Cured T_g

The glass transition temperature was also measured for each of the samples after being fully-cured. The average value for the fully-cured sample group was 109.37°C and the data ranged between 90.90°C and 116.54°C. A histogram is provided in Figure 15 to summarize this data. Contrary to the initial T_g values, the data set for the fully-cured T_g values appears to have less variance and it is likely that the thermal properties for each of the epoxy coatings are similar to one another, regardless of the bridge structure's time of construction and manufacturing conditions.

Figure 15 Histogram of Fully-Cured T_g (C°)

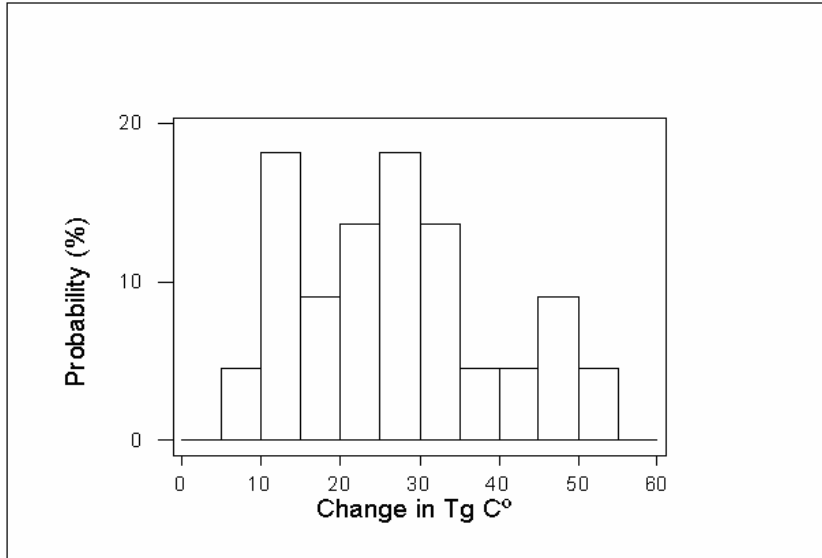


Min:	90.90
1st Qu.:	103.97
Mean:	109.37
Median:	112.89
3rd Qu.:	114.55
Max:	116.54
Total N:	22
StDev:	6.83

Change in T_g

The change in T_g was determined for each sample by noting the difference between the initial T_g and fully-cured T_g . Figure 16 presents the difference in values with a histogram where the average temperature change in T_g is 26.77°C and the data ranges between 5.86°C and 50.01°C . It can be seen from the change in T_g data that none of the samples tested have reached a fully-cured T_g at the time of bridge construction.

Figure 16 Histogram of Change in T_g ($^\circ\text{C}$)

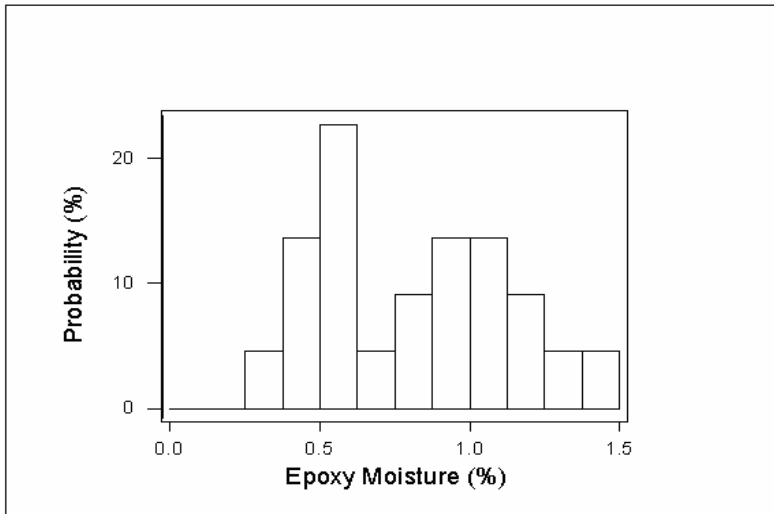


Min:	5.86
1st Qu.:	16.64
Mean:	26.77
Median:	26.99
3rd Qu:	34.12
Max:	50.01
Total N:	22
StDev:	13.08

Epoxy Moisture Content

The epoxy moisture for the 22 sample subset of the previous study averaged 0.81% and ranged between 0.33% and 1.39%. The histogram for this data is presented in Figure 17.

Figure 17 Histogram of Epoxy Moisture Content (%)

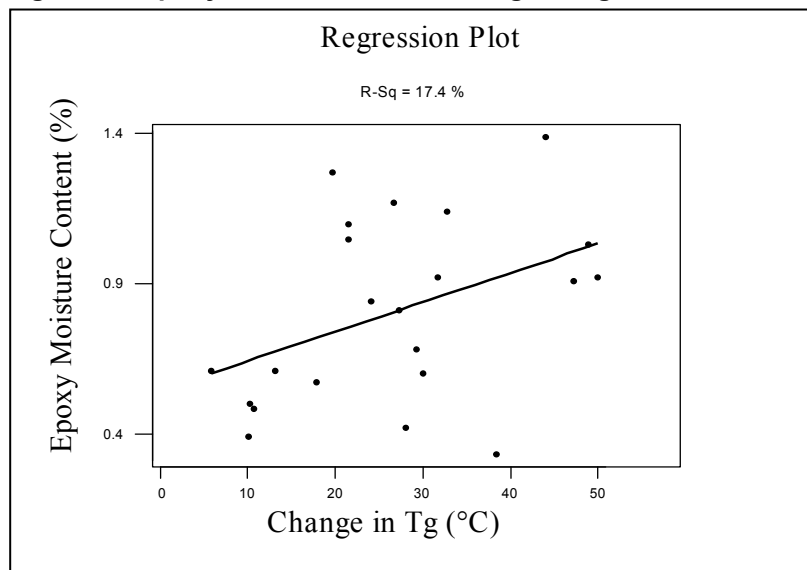


Min:	0.33
1st Qu.:	0.55
Mean:	0.81
Median:	0.83
3rd Qu:	1.06
Max:	1.39
Total N:	22.00
StDev:	0.31

Epoxy Moisture Content versus Change in T_g

The moisture content for each of the samples was examined while considering its corresponding change in T_g . The correlation considers the 22 specimens that were selected for testing from the previous study. The percent moisture was plotted against the change in T_g in Figure 18 and a correlation with a R^2 value of 0.17 and a p-value of 0.053 was revealed. The correlation indicates that the greater the change in the T_g , the more likely the sample will absorb moisture. This is to be expected because lower initial T_g values indicate a lower molecular weight and this provides a greater amount of free volume for a given sample to absorb moisture.

Figure 18 Epoxy Moisture versus Change in T_g



Crack Frequency & Crack Width

The crack frequency was rated for each of the samples on a scale of 1 through 4, representing surfaces that exhibited zero cracking to severely cracked surfaces, respectfully. The largest group of specimens was classified with a crack frequency rating of 1 and the least amount of specimens was rated by a 4. This data is presented in a histogram in Figure 19.

The crack width was also observed for some of the severely cracked coating for ECR samples. Figure 20 shows a SEM photograph magnified at 10K for a specimen from the 1019 bridge. The crack width was measured at two locations and had an average of $1.962\mu\text{m}$. The crack width damage indicates that the epoxy coating surface could easily

permit moisture and chloride ions to penetrate to the steel surface when considering that a water molecule is several orders of magnitude lower, measuring approximately $9.85 \times 10^{-5} \mu\text{m}$ (0.985 \AA) in width and a chloride ion is $3.62 \times 10^{-4} \mu\text{m}$ (Jones, L. & Atkins, P., 2000).

Figure 19 Histogram of Crack Frequency

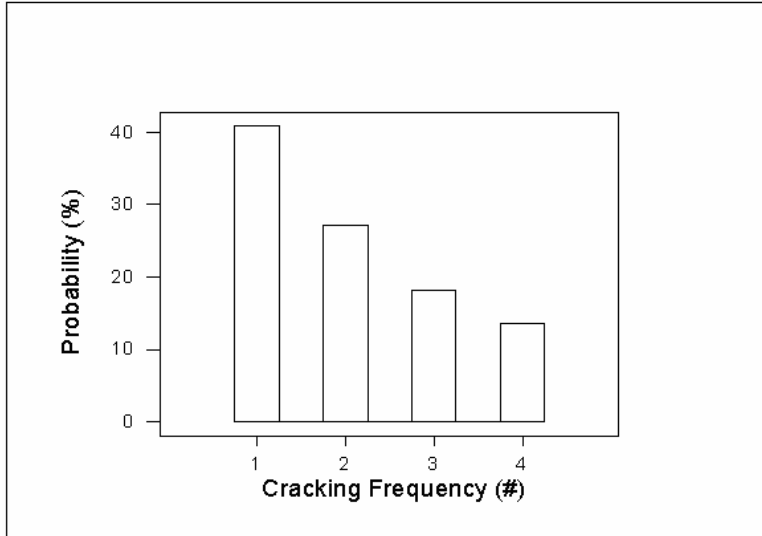
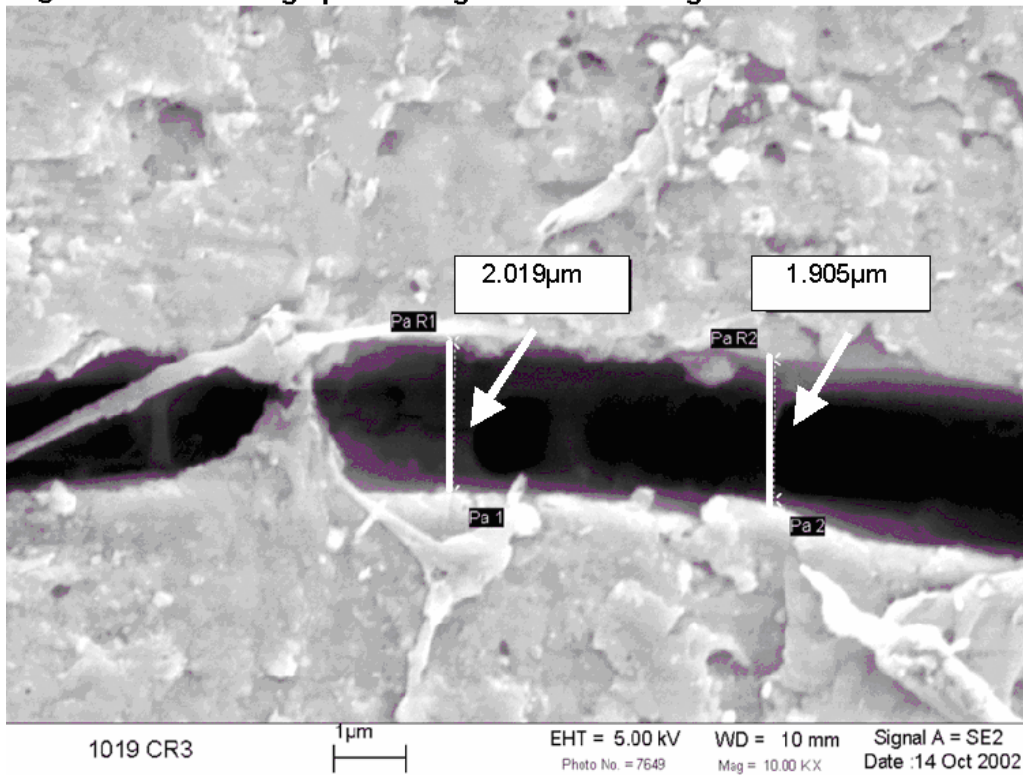


Figure 20 SEM Photograph 10K Magnification Showing Crack Width Measurements

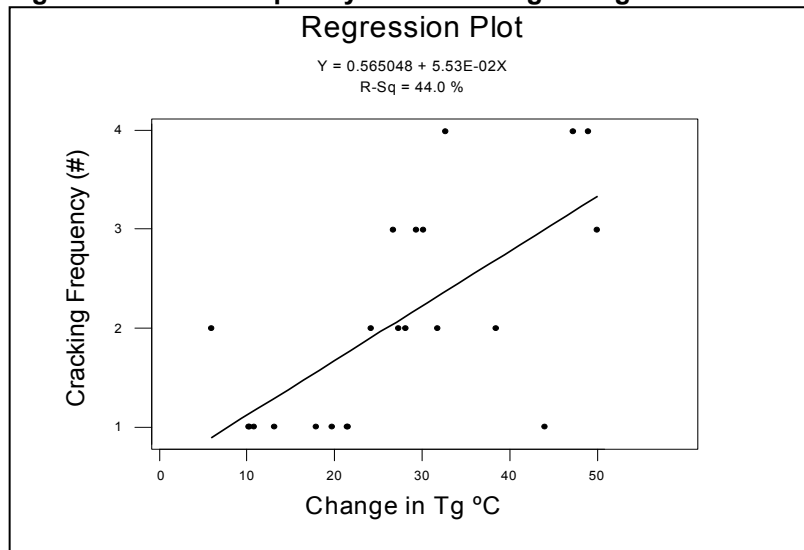


Crack Frequency versus Change in T_g

The relationship between the crack frequency and the change in T_g were plotted in Figure 21 with a R^2 value of 0.44 and a p-value of 0.001. The data for this relationship was determined from the 22 sample set of the previous study. It reveals that when a sample has a greater change in T_g , it has a higher likelihood of exhibiting surface cracks. Figure 7 in the Results section presents typical ratings for SEM photographs with a 2K magnification. The epoxy surface was measured on a scale of 1 to 4 where 1 represented no surface cracking and 4 represented a severely cracked surface. The linear relationship shown in Figure 21 offers a more precise prediction of the cracking frequency, ranging between the ratings 1 through 4, when the change in T_g for the epoxy is known. For example, based on the data of the 22 sample set, the model equation $y = 0.0553x + 0.565$, can predict (with an accuracy of 44%) that an epoxy having a Change in T_g value of 40°C may have a cracking frequency of approximately 2.77 ($= 0.0553*40 + 0.565$). While the original scale of the measurements is on an ordered categorical scale, we can interpret these non-integer values as having an expected level of cracking between categories 2 and 3, with an observed amount of cracking closer to category 3.

The results for this correlation are reasonable because it is likely that the epoxy coating will be more vulnerable to cracking if it is not fully-cured. The epoxy coating surface cracks were examined using SEM and, based on their orientation, demonstrated that an unstable channeling process has taken place, as shown in Figure 7 of the Results section. Also, the literature states that the channeling process can take place as contraction strains occur within the film as it undergoes thermal transitions (Hutchinson, J.W., 1992). Applying this concept to ECR explains that the channeling process may be prompted when thermal transitions are providing a driving force that exceeds the elastic strain energy required by the epoxy to resist cracking. The changes in T_g indicate that the epoxy network is not fully developed and this would cause the weaker coatings to be more susceptible to channeling processes. It should be emphasized that all ECR specimens tested in this study have been subjected for a minimum of 4 years to regular thermal transitions, such as freeze-thaw cycles, that reflect the typical field conditions in the state of Virginia.

Figure 21 Crack Frequency versus Change in Tg



Section Three: Determining Corrosion Initiation Time and Cracking Time from Epoxy and Concrete Parameters

Comparing Initiated, Non-Initiated, and Cracked Specimens

Attempts were made to identify parameters that explain the differences between initiated, non-initiated, and cracked specimens. The parameters considered included bar color, adhesion, thickness, holidays, and percent moisture for the epoxy coating. The diffusion coefficient, the percentage of void saturation, and the chloride concentration at the times of initiation and cracking were also evaluated using concrete encasing the ECR at bar depth. The mean sample size of the parameters investigated was limited for various reasons. Only truncated specimens could be considered in evaluating non-initiated and initiated specimens. Furthermore, specimens from the present study could only be considered if supporting information was available from the previous studies made by Pyc and Brown.

The data summary for coating and concrete parameters is presented in Table 16. Pairwise comparisons were used to compare the means of each of the parameters among the three specimen groups; initiated, non-initiated, and cracked. None of the t-tests yielded significant differences between the groups for any of the parameters tested. Ultimately, based on the available data, none of the individual parameters could be used to effectively classify the specimens into three groups.

Table 16 ECR Data Summary for Coating and Concrete Parameters

Classification	Bridge	#	(Data obtained from Previous Study by Pyc)				Epoxy Moisture (%)	Chlorides at Autopsy (kg/m ³)	% Saturation in Concrete Voids (%)	Diffusion Coefficient (mm ² /yr)	Chlorides at Initiation (kg/m ³)
			Adhesion (#)	Bar Color (#)	Thickness (µm)	Holidays (#)					
Non Initiated/ Not Cracked	1136	C3	1	0	244	1	1.06	7.78	75.08	-	-
	1136	C10	1	0	172	0	0.82	2.60	85.91	79	-
	1004_6	C4	3	4	256	0	2.10	11.83	90.51	347	-
	1004_6	C10	5	4	240	0	1.22	10.82	86.99	543	-
	1001	C3	2	1	260	2	1.01	21.45	77.21	-	-
	1001	C5	5	4	260	2	1.13	9.53	79.42	96	-
	1001	C6	2	1	210	3	1.07	8.82	91.33	72	-
	1001	C7	1	0	180	1	0.89	8.26	73.40	51	-
	1019	C3	5	4	138	0	1.05	14.26	98.41	-	-
	1019	C5	4	4	169	0	0.97	15.29	74.83	-	-
	1019	C8	5	4	168	0	1.12	11.50	92.80	5558	-
	1004_3	C6	1	0	253	2	0.83	10.85	98.14	-	-
	1004_3	C7	1	0	192	3	0.33	13.14	76.53	3861	-
Average			2.77	2.00	210.92	1.08	1.05	11.24	84.66	1325.88	-
StDev			1.72	1.88	41.42	1.14	0.37	4.28	8.71	2005.42	-
CoV (%)			61.99	94.05	19.64	105.95	35.53	38.10	10.29	151.25	-
Initiated/ Not Cracked	1004_6	C5	5	4	240	0	1.24	9.04	89.02	-	-
	1019	C2	5	4	146	0	1.09	15.26	96.44	-	-
	1019	C6	4	4	172	0	1.17	17.65	89.02	-	-
	1015	C2	2	3	215	0	0.88	12.39	96.43	1716	12.33
	1015	C5	5	4	154	3	1.09	11.67	96.10	-	-
	1015	C7	1	1	257	3	0.59	14.46	92.38	543	3.8
	1004_3	C2	2	3	154	4	1.24	12.77	98.94	145	4.36
	1004_3	C11	1	0	170	2	0.97	9.66	95.84	-	-
	2021	C2	5	4	192	1	1.21	13.62	66.84	-	-
	2021	C3	1	4	273	2	0.99	9.47	74.90	206	6.58
	2021	C9	5	4	223	2	1.56	15.39	95.14	-	-
	2021	C12	4	4	197	3	1.06	10.40	93.07	429	9.21
	Average			3.33	3.25	199.42	1.67	1.09	12.65	90.34	607.80
StDev			1.78	1.36	42.46	1.44	0.23	2.73	9.73	640.29	3.55
CoV (%)			53.26	41.75	21.29	86.13	21.52	21.55	10.77	105.35	48.90
Cracked	1136	C7	1	0	301	0	1.05	7.73	-	108	0.08
	1004_6	C7	5	4	229	2	0.60	9.52	-	253	0.74
	1004_6	C11	1	0	278	0	0.42	6.38	-	-	-
	1001	C2	5	4	219	7	0.50	10.87	-	-	-
	1015	C1	5	4	339	2	0.92	9.96	-	158	8.48
	1015	C10	1	0	227	0	0.81	13.18	-	2071	8.46
	2262	C8	4	3	139	0	1.03	10.48	-	192	0.71
	2262	C10	1	1	157	1	0.91	9.85	-	8511	9.31
	1004_3	C1	2	1	167	2	0.33	9.6	-	-	-
	1004_3	C3	1	0	170	2	1.27	9.78	-	-	-
	2021	C6	1	1	238	1	0.61	6.29	-	-	-
Average			2.45	1.64	224.00	1.55	0.77	9.42	-	1882.17	4.63
StDev			1.86	1.75	63.41	2.02	0.30	2.00	-	3334.92	4.53
CoV (%)			75.92	106.81	28.31	130.58	38.69	21.20	-	177.18	97.84

Parameters Influencing Time to Corrosion Initiation

The time to corrosion initiation was initially investigated by considering the pairwise correlation matrix to determine which variables had the highest statistical influence on this time period. The parameters investigated included adhesion, holidays, thickness, and percent moisture for the epoxy coating, while the diffusion coefficients and chlorides at corrosion initiation were examined for the concrete using the data in Table 16. The data for the correlation matrix was limited to only the initiated and cracked categories and only when diffusion coefficient values were available. Although the relationship between each parameter and its corresponding time to corrosion initiation was the focus (these values are highlighted in Table 17), the matrix also established the relationships among

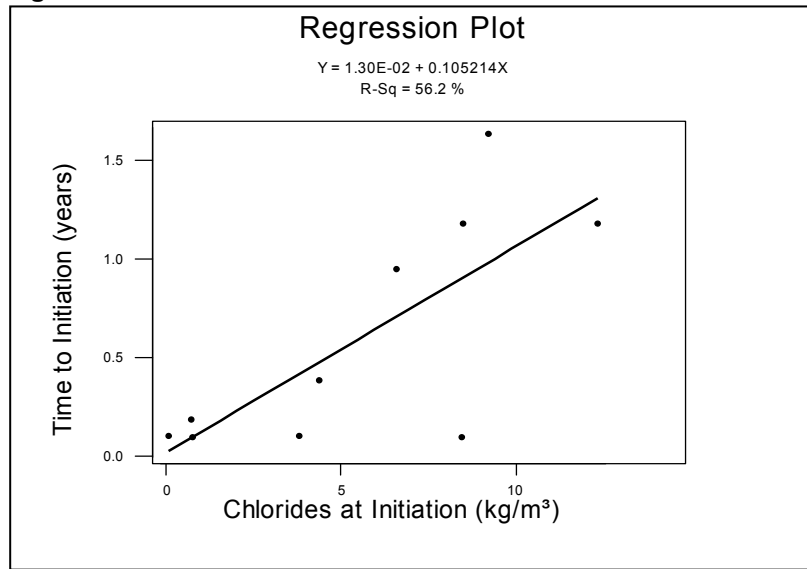
the individual parameters. The results for the correlation matrix are presented in Table 17, where information for the statistical significance of any two variables can be established by noting the correlation value (R), the sign convention for the correlation value, along with its corresponding p-value. Absolute correlation values closer to 1 (rather than 0) will imply a stronger relationship. In regards to the sign convention for the correlation between any two variables, a positive sign explains a direct relationship while a negative sign depicts an inverse relationship. Finally, the p-value determines if the correlation value is highly significant (< 0.01), significant ($\geq 0.01, < 0.05$), marginally significant ($\geq 0.05, < 0.1$), or not significant (≥ 0.1). For example, the correlation matrix revealed that the most highly influential variable for determining the time to corrosion initiation was the chloride concentration at bar depth at the time of initiation. The square of the correlation value, 0.750, yields an R^2 of 56.2%, and the p-value of 0.013 justifies that the R^2 value is significant. Finally, the positive sign convention indicates that higher levels of chloride correlate to increasing time to corrosion initiation (a negative sign would indicate higher levels of chloride are matched with decreasing times to corrosion initiation). In addition, the correlation of 0.616 between diffusion coefficients and chlorides at initiation has a marginally significant relationship. This relationship is expected because the diffusion coefficient value was used to estimate the value of chlorides at the time of corrosion initiation, as seen in Equation 1 of the Results section.

Table 17 Correlation Matrix for time to corrosion initiation and epoxy & concrete parameters. Correlation values in bold and p-values in parentheses

	Adhesion	Thickness	Holidays	Moisture	Diffusion	Chlorides
Thickness	-0.084 (0.817)	note: p-value $\in [0.05, 0.1]$, marginally significant p-value $\in [0.01, 0.05]$, significant p-value < 0.01 , highly significant				
Holidays	0.147 (0.686)	-0.083 (0.82)				
Epoxy Moisture	-0.064 (0.861)	-0.298 (0.403)	0.093 (0.799)			
Diffusion rate	-0.361 (0.305)	-0.112 (0.758)	-0.477 (0.163)	-0.292 (0.413)		
Chlorides at Initiation	-0.066 (0.856)	0.100 (0.783)	0.008 (0.982)	0.062 (0.864)	0.616 (0.058)	
Time to Initiation	0.295 (0.408)	0.132 (0.716)	0.220 (0.541)	0.320 (0.367)	0.120 (0.973)	0.750 (0.013)

Once the chloride concentration was recognized as the greatest predictor for the time to corrosion initiation, a linear regression analysis was performed and the results are presented in Figure 22. Knowing the time to corrosion initiation and applying this value to the linear regression equation, $y = 0.105x + 0.013$, explains 56.2% of the variability for the time to initiation values.

Figure 22 Time to Initiation versus Chlorides at Initiation



Parameters Influencing Time to Corrosion-Induced Cracking

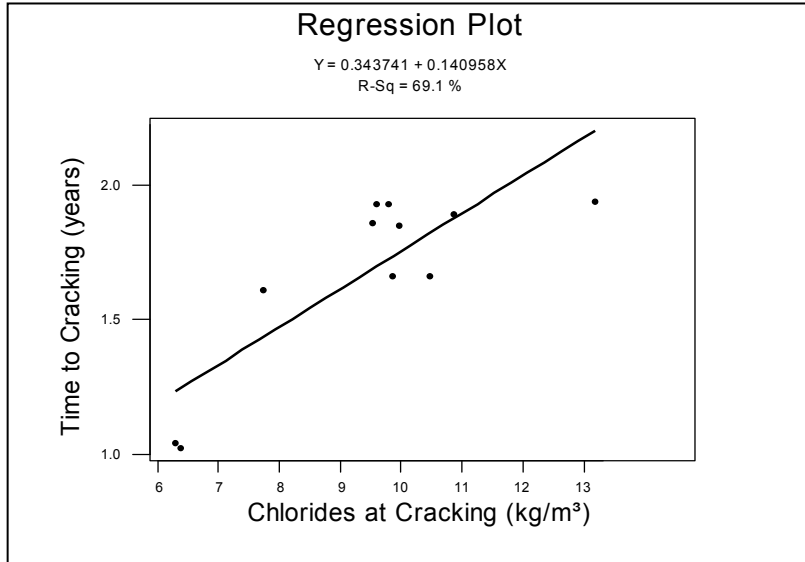
The time to corrosion-induced cracking was analyzed by observing the effect that a variety of concrete and epoxy parameters had on it. The relationships among the time to corrosion-induced cracking and the epoxy and concrete parameters were investigated by examining the correlation matrix, as seen in Table 18. Only data from the cracked category of Table 16 was available while the diffusion coefficient was omitted because the sample size was too small. Altogether, the epoxy variables included adhesion, thickness, holidays, and percent moisture while the concrete variables involved the chloride concentration at bar depth at the time of cracking. Determining the correlation between the time to cracking and the parameters are the main objective for this matrix (these value are highlighted) and the matrix also displays the relationship that the parameters have among each other. The procedure for interpreting the statistical significance of the matrix is identical to the methods discussed in the previous section, Parameters Influencing Time to Corrosion Initiation. The correlation matrix revealed that the strongest predictor for determining the time to corrosion-induced cracking is chloride concentration at bar depth. The square of the correlation value, 0.831, produces an R^2 of 69.1% and the 0.002 p-value validates the R^2 value as highly significant. The positive sign for the correlation value between chloride concentrations and times to corrosion-induced cracking explains that higher chloride concentrations coincide with increasing time to corrosion-induced cracking. In other words, ECR that requires higher levels of chlorides for corrosion-induced cracking will, respectively, take longer amounts of time until cracking takes place.

Table 18 Correlation Matrix for time to corrosion cracking and epoxy & concrete parameters. Correlation values in bold and p-values in parentheses

	Adhesion	Thickness	Holidays	Moisture	Chlorides	Initiation time
Thickness	0.125 (0.714)		note: p-value € [0.05,0.1], marginally significant p-value € [0.01,0.05], significant p-value < 0.01, highly significant			
Holidays	0.566 (0.7)	-0.055 (0.873)				
Epoxy Moisture	-0.143 (0.675)	-0.080 (0.815)	-0.300 (0.37)			
Chlorides at Cracking	0.314 (0.347)	-0.332 (0.319)	0.243 (0.472)	0.228 (0.501)		
Initiation time	0.364 (0.271)	0.282 (0.401)	0.534 (0.09)	0.164 (0.63)	0.112 (0.742)	
Cracking time	0.406 (0.216)	-0.254 (0.451)	0.387 (0.239)	0.267 (0.427)	0.831 (0.002)	0.207 (0.541)

Next, a linear regression analysis was considered for predicting the time to corrosion-induced cracking from the chloride concentration level and the results are presented in Figure 23. Knowing the chloride concentration level and applying it to the equation, $y = 0.141x + 0.344$, explains 69.1% of the variability of the time to corrosion-induced cracking values.

Figure 23 Time to Cracking versus Chlorides at Cracking



CONCLUSIONS

The following conclusions can be drawn from the results of the present study:

There is no significant difference between the bare steel and ECR populations tested in this study when considering the estimated chloride concentrations at the time of corrosion initiation. Essentially, it requires the same amount of chloride concentration to initiate corrosion for bare steel that it does for ECR specimens. This means that the ECR population did not provide any advantage to bare steel in preventing chloride-induced corrosion on the steel's surface when exposed to chloride ions.

The epoxy coating for ECR samples selected for testing did not exhibit fully-cured glass-transition temperatures and, therefore, the coatings were not cured to their fullest extent at the time of highway bridge construction.

The greater the change between an epoxy's initial T_g and its fully-cured potential correlates to an increase in cracking in the epoxy coating.

Development of cracking can occur in the epoxy coating to the extent where crack widths exceed the size of water molecules and chloride ions by several orders of magnitude.

There is no significant difference between epoxy coating and concrete parameters when classifying ECR specimens into three separate populations; those that have (1) not initiated corrosion, (2) initiated corrosion without cracking, or (3) initiated corrosion leading to concrete surface cracks.

The amount of chloride that accumulates at bar depth is the strongest indicator for predicting the time to corrosion-initiation and corrosion-induced cracking.

RECOMMENDATIONS

Alternative methods for corrosion prevention should be investigated for replacing ECR. Attention should be paid to enhancing concrete conditions to reduce diffusion of chloride ions.

The thermal properties of the epoxy coating for ECR should be investigated subsequent to manufacturing and prior to bridge construction.

Methods for enhancing the curing conditions for ECR should be investigated.

Specifications should be made, perhaps under ASTM Standards to control T_g during ECR curing so that coatings are developed to their full potential.

Changes of thermal properties over time should be evaluated for ECR. Particularly, testing should be conducted for ECR prior to bridge construction and compared to conditions after being employed in bridge decks for an extended period of time. The testing should include the T_g , the moisture content, and the crack frequency in the epoxy coating.

ACKNOWLEDGEMENTS

I would especially like to thank my advisor, Dr. Richard Weyers, for investing his trust in me and for providing me with such a truly enriching research experience.

I would like to thank Dr. Michael Brown for committing himself to this project and for mentoring me and, also, Dr. Christine Anderson-Cook for being a member of my committee and for her constant support and guidance.

Appreciation is also extended to Mr. Michael Sprinkle and the Virginia Transportation Research Council for sponsoring, funding, and providing their resources throughout this project.

I would also like to acknowledge, with deep gratitude, Professor Siegfried Holzer for his support and encouragement during a time of need.

Thank you, also, to Michael Sumner for offering his expertise in polymer chemistry and to Steve McCarthy for his assistance with microscopy.

I would like to thank my friends Julie Harding, Kate Harding, Timmy Hays, Alicia Karwoski, and Ed Vincent for their loyal support.

Finally, I can not thank my parents enough for extending their love and confidence in me to succeed.

REFERENCES

“National Transportation Statistics 2000”. 2001. Bureau of Transportation Statistics (BTS) of the U.S. Department of Transportation. 2001.

Brown, Michael C., “Corrosion Protection Service Life of Epoxy Coated Reinforcing Steel in Virginia Bridge Decks”, Dissertation in Civil and Environmental Engineering, Virginia Polytechnic Institute & State University, Blacksburg, VA, 2002.
<http://scholar.lib.vt.edu/theses/available/etd-05132002-120642/>.

Clifton, J.R., H.F. Beeghly, & R.C. Mathey, “Nonmetallic Coatings for Concrete Reinforcing Bars”, Report No. FHWA-RD-74-18, Federal Highway Administration, Washington, D.C., 1974.

FHWA, The Status of the Nation’s Highway Bridges: Highway Bridge Replacement & Rehabilitation Program & National Bridge Inventory, “Thirteenth Report to the U.S. Congress, Federal Highway Administration, Washington, D.C., 2002.

Jones, L. & P. Atkins, *Chemistry; Molecules, Matter, and Change*. 4th ed. New York: W. H. Freeman and Company, 2000.

Koch, G.C., M.P. Brongers, N.G. Thompson, Y.P. Virmani, & J.H. Payer. “Corrosion Costs and Preventive Strategies in the United States”. Report No. FHWA-RD-01-156. Federal Highway Administration, Washington, D.C., 2002.

Manning, D.G., “Corrosion Performance of Epoxy-Coated Reinforcing Steel: North American Experience”, *Construction and Building Materials* v. 10n. (5), 349-365. 1996.

McKeel, W.T., Jr, Evaluation of Epoxy-Coated Reinforcing Steel.1977. Charlottesville, VA, Virginia Transportation Research Council.

Pyc, Wioleta, “Field Performance of Epoxy-Coated Reinforcing Steel in Virginia Bridge Decks”, Virginia Polytechnic Institute & State University, 1998.

Rieger, Philip H. *Electrochemistry*. 2 ed. New York & London: Chapman & Hall, 1994.

Virmani, Y.P., K.C. Clear, & T.J. Pasko, “Time-to-Corrosion of Reinforcing Steel in Concretes”, Vol. 5: Calcium Nitrite Admixture or Epoxy-Coated Reinforcing Bars as Corrosion Protection Systems.” Report No. FHWA/RD-83/012, Federal Highway Administration, Washington, D.C., 1983.

APPENDICES

APPENDIX A: LITERATURE REVIEW

A thorough summary for the research concerning this work is available in the literature review from the previous study by Brown (Brown, M. C., 2002). The following presents a brief overview of all pertinent topics from his research, and includes an update of the most recent articles published concerning ECR. Also, information on epoxy polymers and their testing methods are included in this section relative to the additional testing that was conducted in the present study.

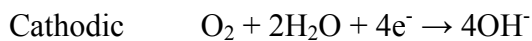
Corrosion of Steel in Concrete

The Passive State

The passive state is the ideal environment in which steel in concrete is protected from corrosion. Passivity occurs in a high pH (approximately 12 to 13) medium and when water and oxygen are both provided (Schiessl, P., 1983). This high alkaline environment causes a protective surface layer to naturally form on the steel's surface. When this film remains undisturbed and in its passive state it is able to protect the steel from corroding (St. John, D. A., Poole, A. B., & Sims, I., 1998).

Mechanism for Corrosion of Bare Steel in Concrete

Steel corrodes in concrete through an electrochemical process that includes two chemical reactions along with an electrical current that flows between them. The two reactions are known as anodic and cathodic and they react simultaneously to one another on the steel's surface. The anodic reaction involves the loss of metal that takes place during the corrosion process where iron atoms ionize to ferrous ions. The ferrous ions dissolve into the water solution retained in the pores of the surrounding concrete. Released electrons then flow to areas of the steel that have lower potentials, which are known as cathodic sites. At these locations, water and oxygen molecules react with the electrons and hydroxide (OH⁻) ions are formed. The basic formulas for the anodic and cathodic reactions that take place are as follows (Brown, M. C., 2002):



Collectively, the two reactions take place at the same rate; hydroxide ions travel from the cathode to the anode in exchange for the electrons to the cathode site. The reactions are synchronized so that the anodic reaction will take place when oxygen and water are present while an electrical current path is provided by the steel bar (Bentur, A., Diamond, S., & Berke, N. S., 1997). Reactions take place between the ferrous (Fe²⁺) and the hydroxide (OH⁻) ions and, as a result, ferrous hydroxide, Fe(OH)₂, forms. If this corrosion compound continues to undergo additional reactions with oxygen, rust formation can occur and is most commonly seen as red rust, Fe₂O₃, or black rust, Fe₃O₄.

Chloride-Induced Corrosion

One of the more common methods for steel corrosion in concrete to occur is when a critical level of chloride ion concentration develops at the steel's surface through the presence of chloride salts (Berke, N. S. et al., 1996). If deicing salts are applied to the concrete bridge's pavement surface, the chloride ions can travel to the steel's surface as they diffuse through a pore solution that is within the concrete. Once the chloride ions reach the steel surface, they can break down the protective passive layer by reacting with the iron complex. Iron-chloride compounds (FeCl_2) are formed and can react with additional hydroxide ions. The result is the formation of white ferrous hydroxide ($\text{Fe}(\text{OH})_2$) which can further react with hydroxide ions to form either red-brown or black rust by-products.

Corrosive Reactions of Reinforced Concrete Specimens

A variety of corrosion reactions can take place throughout a reinforced concrete specimen that coincides with each other (Brown, M. C., 2002). To begin with, macrocell corrosion can occur as a result of varying levels in potential values among individual reinforcing steel bars within the concrete at varying depths. Cathodic sites form on bars that have lower levels of chloride concentration which can chemically react with the bars containing higher chloride concentrations, acting as anodic sites. Microcell corrosion can also take place for individual steel bars when neighboring anodic and cathodic sites form as a result of varying levels of chloride concentration throughout its surface. Pitting corrosion is a particular type of microcell corrosion that is common for chloride-induced corrosion. Pitting corrosion occurs when anodic sites form at pits on the steel's surface that contain a highly concentrated chloride environment with lower pH values. Meanwhile, neighboring cathodic areas form on the steel that are in the passive state and corrosively react with the anodic sites.

Chloride Corrosion Threshold

Many factors must be maintained in order for the passive film to remain intact for reinforcing steel that is embedded in concrete and subjected to chloride ions (Crane, A. P., 1983). The corrosion process will take place when a high enough volume of chloride concentration accumulates to destroy the protective film on the steel's surface. This process takes place when the chloride corrosion threshold has been reached, which is the minimum amount of chloride concentration necessary to initiate corrosion in the surrounding concrete (Mietz, J., Polder, R., & Elsener, B., 2002). The chloride corrosion threshold value can vary between different cement types and mix designs for concrete and can be influenced by the pH of the surrounding porewater and ambient temperatures.

A recent study presents data on the influence of both chloride concentration and pH when observing reinforcing steel corrosion. The results showed that the chloride concentration threshold values for corrosion initiation were lower for corresponding values of lower pH and that corrosion takes place regardless of the chloride concentration for all pH values below 11 (Matsushima, I., 2002).

In addition to the significance of the chloride concentration, once the corrosion process is initiated on concrete the rate of corrosion is also influenced by a variety of factors that involve the concrete quality along with the surrounding environment. In another study, data is presented on how the ambient temperature affects the rate of corrosion for reinforcing steel. The results indicated that the corrosion rate tended to accelerate as the ambient temperatures increased (Zivica, V., 2002).

Summary of Corrosion Prevention Methods

A variety of methods are commonly practiced to help delay the corrosion process from occurring in concrete. One technique is to use a high cover depth over the reinforcing steel so that it takes a greater length of time for chloride ions to reach the steel's surface. Another method is to use a concrete that has low permeability so that chloride ions have limited means of diffusing through the porewater solution. Coatings such as zinc can also be applied to the steel rebar as a sacrificial metal to postpone the corrosion process. Also, corrosion inhibitors may be used to increase the chloride corrosion threshold concentration. In addition to these common examples, one of the leading methods for preventing corrosion is to apply an organic epoxy coating to the reinforcing steel bar as a barrier from the chloride ions to the steel's surface (Cramer, S. D, et al., 2002; Neville, A. M., 1996).

ECR

Epoxy Polymers; an Overview

In the field of polymer chemistry, epoxy related polymers are often looked upon as an extremely practical material for many purposes. In addition to their common application in society, epoxies are desirable because they are materials that can be developed with relative ease into a variety of manufactured products. For example, it is possible to fabricate epoxies while controlling their degree of strength and thermal stability (May, C. A., 1988). An overview on the chemical and thermal properties of epoxy material is presented below, which focuses on the basic synthesis and curing reactions that occur during epoxy fabrication.

In general, epoxies are formed by combining an epoxy resin with a curing agent. Together, these materials react chemically as they go through the curing process. These materials can have a variety of chemical structures that are able to cure over a wide range of temperatures so that many different properties can be obtained. As a result, it is possible to develop an epoxy in a controlled environment so that a high quality polymer may be achieved from an abundant range of parameters.

Epoxy polymers are formed when an epoxy resin undergoes a curing process where individual epoxy groups with low molecular weight convert to a highly crosslinked network. This phenomenon is known as a polyaddition reaction. While curing, a highly networked polymer is created as the individual epoxy monomers react among their functional groups. The number of functional groups for a given monomer will determine

the magnitude of networking that takes place in the polymer. This reaction is controlled by the curing temperature and determines the gel point, which marks the transformation of the liquid state to the solid state of a network. Growth and branching generally develop for a polymer chain in the liquid phase while the polymer chains undergo crosslinking (networking) once it reaches the gel point. As the polymer undergoes a cross-linking formation it results in a system that is more complex and yields an increased glass transition temperature (T_g) when the reaction ceases (May, C. A., 1988). Figure 24 displays a schematic representation of polymers at linear, branched, and crosslinked (networked) stages.

Manufacturing ECR

The typical method for manufacturing ECR is by a fusion bonding process where the reinforcing steel bars are heated and an epoxy powder is applied. The steel bars are shot blasted to clean the surface from any impurities and a powder application of the epoxy resin immediately follows (Pyc, W. A. et al., 2000). The powder particles contain an electrostatic charge which naturally attracts to the steel surface as it melts and polymerizes into an adhesive coating.

Glass Transition Temperature

The T_g marks the temperature required for a polymer to lose its solid glasslike structure and to convert into a rubberlike substance as it is heated (Stevens, M. P., 1999). The T_g increases as a polymer network develops because the amount of heat energy that is required to break down the structure rises as a system becomes more complex. For example, in Figure 24, the T_g for part (c.) will be much greater than for part (b).

Characteristics of ECR as a Corrosion Prevention Method

The relationship between elevated crosslinked densities and polymers adhesive properties to a metal surface is presented by Piens and De Deurwaerder. The study examined polyurethane coatings with a variety of cross-linked densities on aluminum surfaces and found that adhesion increased as the cross-linking was elevated (Piens, M. & De Deurwaerder, H., 2001).

Epoxies are prominent for having high quality adhesion and their most popular use has been as protective coatings (Seymour, R. B. & Herman, M. F., 1990). If an epoxy coating has perfect adhesion to a metal surface it should provide corrosion resistance. Ideally, ECR should form a barrier that protects the metal surface from aggressive environmental species. In addition, the coating should also act as an insulator that prevents electrical transfers from taking place.

A recent study analyzed both bare steel and ECR in chloride solutions. It was determined that an epoxy coating handled carefully and applied properly has substantial protection properties that extend service life compared to bare steel for reinforced concrete (Erdogdu, S., Bremner, T. W., & Kondratova, I. L., 2001).

Another recent study exhibited similar results and concluded that fusion-bonded ECR would enhance corrosion resistance in comparison to bare steel and that ECR tested without holidays showed it could provide an adequate barrier to corrosion (Darwin, A. B. & Scantlebury, J. D., 2002).

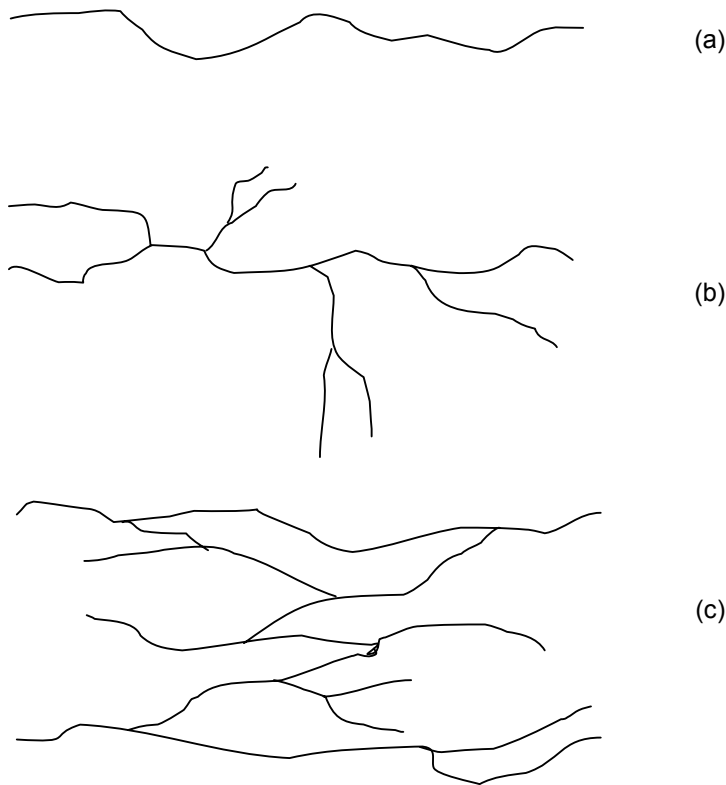


Figure 24 Schematic Representation of Polymers at (a) Linear, (b) Branched, and (c) Cross-linked (Networked) Stages

Damage of ECR

Although it is possible to fabricate ECR that demonstrates excellent adhesion, it is inevitable that ECR will experience surface damage to some degree during the manufacturing process. To begin with, research shows that microscopic impurities remain on the metal's surface even after the shot-blasting, cleaning process is performed. These impurities will yield areas of the ECR that are not fully bonded after the curing process takes place. In response to this problem, standards have been established by

ASTM A 775/A 775M-93 for manufacturing ECR (Bentur, A., Diamond, S., & Berk, N. S., 1997). Some of the most noteworthy requirements are as follows:

- ~ The coating thickness must be between 130 μ m and 300 μ m.
- ~ The total amount of holidays should not be greater than 2 per 0.3m.
- ~ The damage should not exceed 1% of a 0.3m surface.
- ~ The bar must be able to bend about a 152.4mm (6 inch) radius mandrel without forming cracks in the coating.

The problem of adhesion loss during manufacturing has recently been addressed by studies that investigated the effects of using additives in the epoxy coating of ECR. Galliano and Lando found that corrosion inhibiting additives increased the bond strength for waterborne epoxy coatings on the steel's surface (Galliano, F. & Landolt, D., 2002). In addition, another study demonstrates that materials such as river sand can be added to an epoxy to enhance the bond strength between the epoxy and the steel rebar (Chang, J. J., Yeih, W., & Tsai, C. L., 2002).

Although precautions have been taken on limiting damage during ECR manufacturing, additional damage is unavoidable when ECR is used in standard construction procedures (Clear, K. C. et al., 1995).

A study that was performed recently addressed the concern that damage to ECR can not be avoided in the field. It found that defects in the coating develop into additional debondment and corrosion beneath the coating. The ability of ECR to effectively provide corrosion protection is questioned in this report and alternative prevention methods are investigated (Vedalakshmi, R. et al., 2000).

An epoxy coating is naturally permeable to moisture through voids that are present in a polymer network (Leidheiser, H., 1981). If a coating is poorly cured during the manufacturing process of ECR, it is increasingly likely to contain additional voids that are susceptible to moisture. Regardless of the quality of the curing properties of the ECR, the coatings are heterogeneous in nature and variations exist that effect their ability to provide a consistent barrier against moisture. Water can aide in coating debondment both mechanically and chemically (Pyc, W. A. et al., 2000). The water can chemically react with hydroxyl groups found on the steel surface, or the water can mechanically force the coating to undergo blister formation as it accumulates in concentrated regions.

Regardless of the mechanism, once ECR undergoes adhesion loss it has the potential to corrode at any damaged region along the coating's surface.

Corrosion of ECR

Corrosion of ECR is somewhat similar to the corrosion process of bare steel because they both involve development of localized regions where the corrosion reactions take place. Bare steel generally forms pits on the surface, causing pit corrosion, while ECR develops crevices beneath the coating where crevice corrosion takes place. Anodic and cathodic

regions will form beneath the epoxy surface at damaged areas and the corrosion process will proceed in a similar manner to that of bare steel. The primary difference is that hydrogen is reduced instead of oxygen at the cathode site.

Testing Methods

Electrochemical Impedance Spectroscopy

Electrochemical Impedance Spectroscopy (EIS) is a method for measuring corrosion levels by monitoring a potential's amplitude over a wide range of frequencies. The impedance (Z) is expressed as follows (Rossiter, B. W. & Hamilton, J. F., 1986):

$$Z(\omega) = V(t)/I(t), \text{ where}$$

t = time

ω = angular frequency

$$V(t) = V_o \sin \omega t$$

$$I(t) = I_o \sin(\omega t + \theta)$$

θ = phase angle of $V(t)$ and $I(t)$.

Measurements are made by applying a sinusoidal voltage, $V(t) = V_o \sin \omega t$, to a cell and this produces a sinusoidal current, $I(t) = I_o \sin(\omega t + \theta)$, that has an equivalent frequency but is shifted in time by a phase shift, (θ).

Next, the absolute impedance value, $|Z|$, and the phase angle can be measured from the impedance values of its resistance and its capacitance (Gileadi, E., 1993). The resistance is an actual value while the capacitance is accounted for by an imaginary number. Combining the real and imaginary values yields the following complex number:

$$Z(\omega) = \text{Re}Z - \mathbf{j}(\text{Im}Z), \text{ where}$$

$$\mathbf{j} = (-1)^{1/2}$$

One method for plotting the electrode impedance over a range of frequencies is using a Nyquist plot where $-\mathbf{j}(\text{Im}Z)$ is a function of $\text{Re}Z$. Another approach can be done by using a Bode plot, where the $\log |Z|$ and $\log \theta$ are plotted against $\log \omega$. Examples of idealized Nyquist and Bode plots are presented in Figure 25.

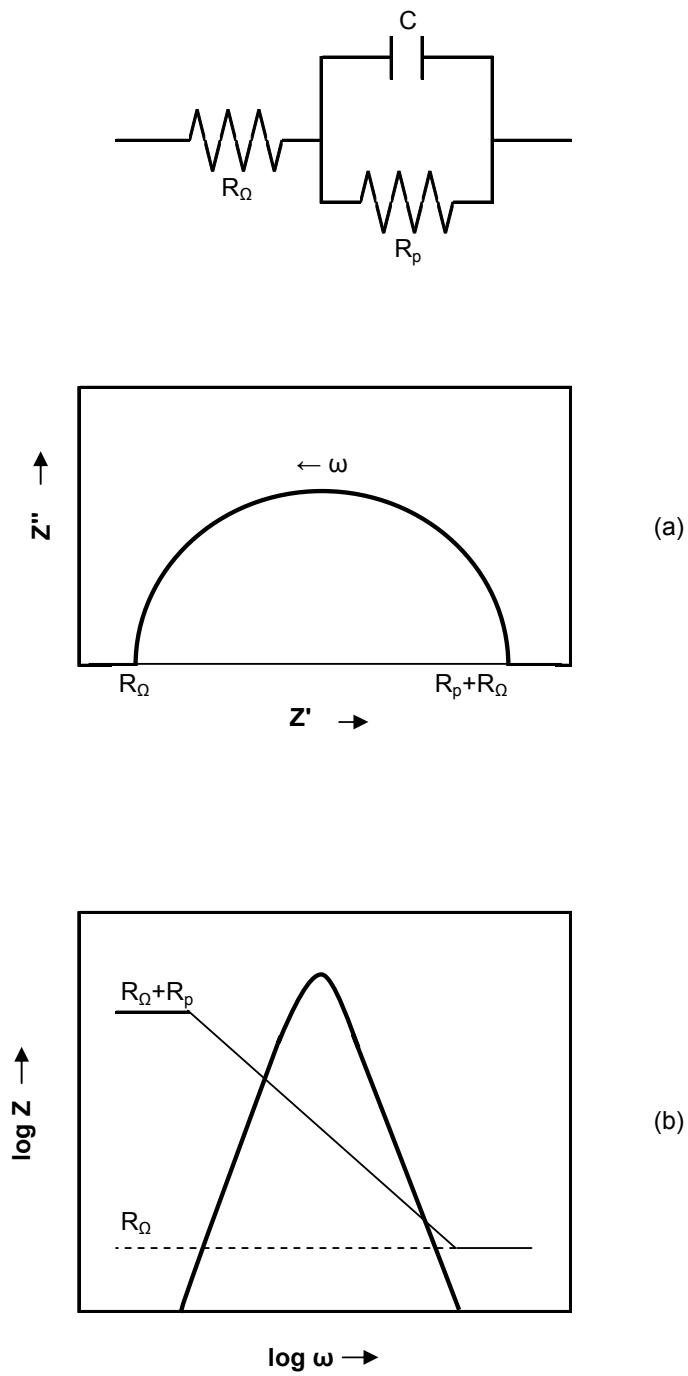


Figure 25 Electrochemical Impedance Spectroscopy Schematic Data Display for a Corroding Electrode by both Parallel-Connected Resistance R_p and Capacitance C : (a) Nyquist Plot (b) Bode Plot

The Nyquist plot tracks the frequency measurements as they increase in a counterclockwise direction. This plot reveals that the imaginary value is nonexistent at extremely high and extremely low frequencies. The highest frequency will measure just the ohmic resistance, R_{Ω} , while the lowest measures the summation for the solution resistance, R_{Ω} , and the polarization resistance, R_p .

A Bode plot presents the same results but in a different fashion. The capacitance is seen as a linear -1 slope and the phase angle, θ , will have a maximum value.

Regardless of the plotting method, the corrosion rate is inversely proportional to the polarization resistance, R_p . The R_p can be obtained by subtracting R_{Ω} from $R_p + R_{\Omega}$, which yields a value that disregards the ohmic resistance. EIS uses a potentiostat at a variety of frequencies where the impedance and phase angle are measured.

Differential Scanning Calorimetry

Differential scanning calorimetry (DSC) is used to measure thermal transitions that occur in polymers during temperature changes (Bershtein, V. A. & Egorov, V. M., 1994). The thermal transitions are detected for a polymer sample that is compared to a reference (Mathot, V. B. F., 1994). The sample and reference systems are both heated with individual heating systems that are both monitored to keep the sample and reference temperatures identical. Figure 26 shows a model for a typical DSC system.

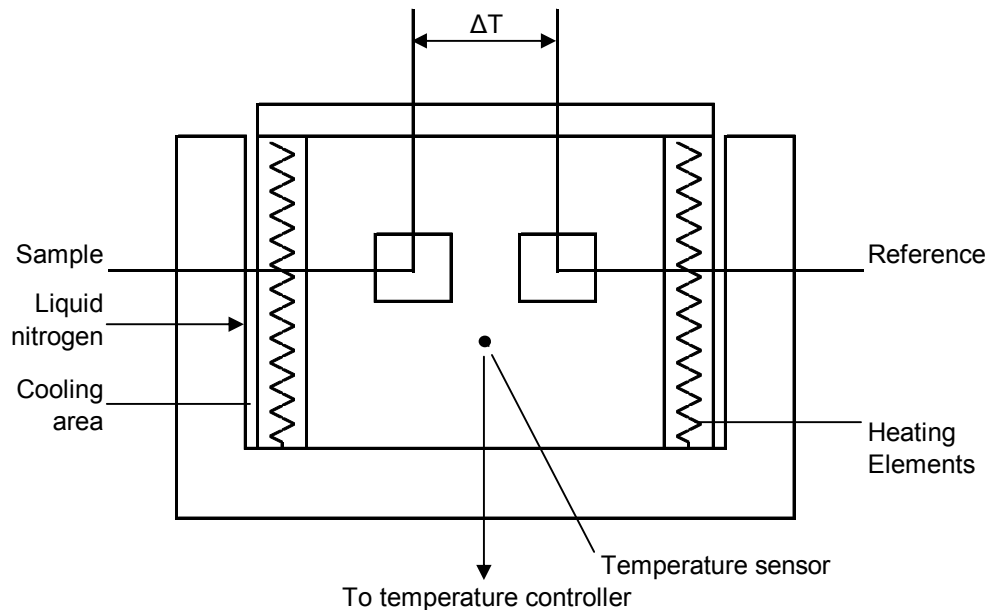


Figure 26 Schematic Representation of a Typical DSC System

The difference in the amount of electrical power ($d\Delta Q/dt$) that is required for either system is measured and noted as temperatures are elevated on plots that are known as thermograms. Thermograms plot both endothermic and exothermic trends that can be used to interpret a polymer's enthalpy, which measures the amount of heat it contains per unit mass (Stevens, M.P., 1999).

Figure 27 is an example of an idealized thermogram where the enthalpy for a sample is plotted temperatures are increased from room temperature to values beyond the boiling point of water, approximately 100°C. Changes in enthalpy are noted at (A) the T_g , (B) crosslinking, and (C) vaporization.

The T_g is detected by an endothermic trend (A) where additional energy is required for the solid (or glasslike) state of the polymer to break down to its rubber state. There is a

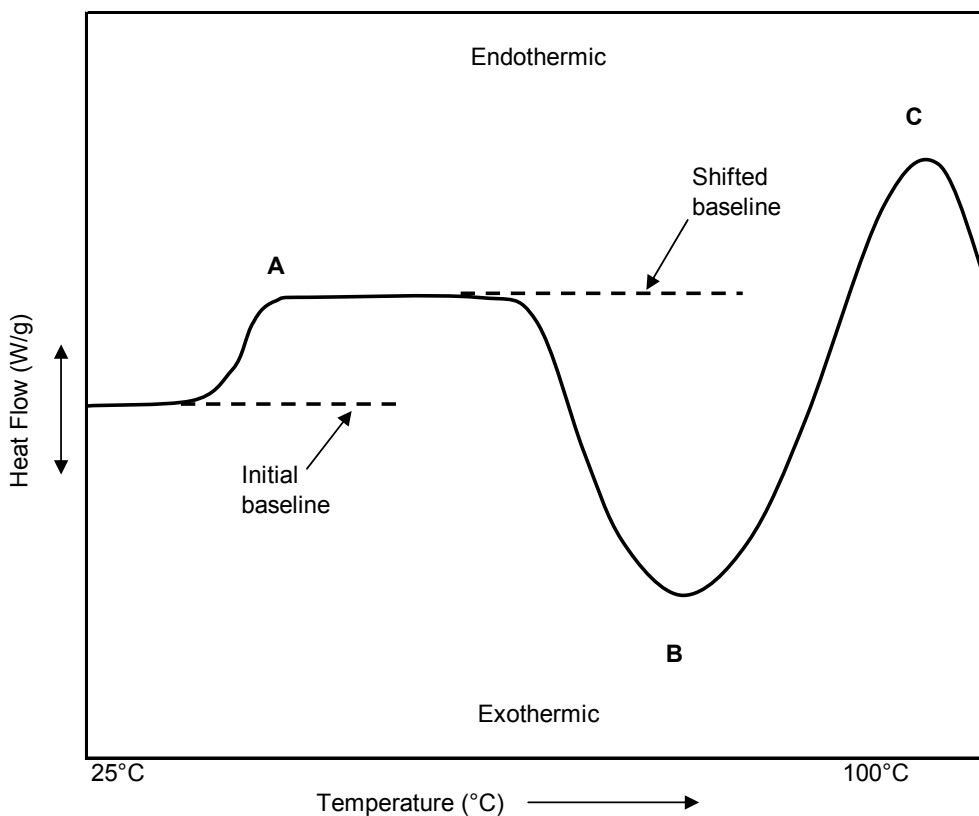


Figure 27 Idealistic Thermogram (marking (A) glass transition temperature, (B) crosslinking, and (C) vaporization) as temperatures are elevated from room temperature to values beyond the boiling point of water.

corresponding shift in the baseline because the heat capacity of the sample has increased while the rubber state for the polymer sample is maintained. The exothermic trend (B) marks the point where a sample continues to cure as crosslinking occurs at unreacted

sites. There is a decrease in the slope because energy is released as these chemical reactions take place. Another endothermic trend (C) occurs as moisture vaporizes when the temperature reaches the boiling point of water. There is an increase in slope because additional energy is required to vaporize any moisture retained by the sample.

Temperature transitions are measured by noting the onset (A) and the offset (B), as indicated in Figure 28.

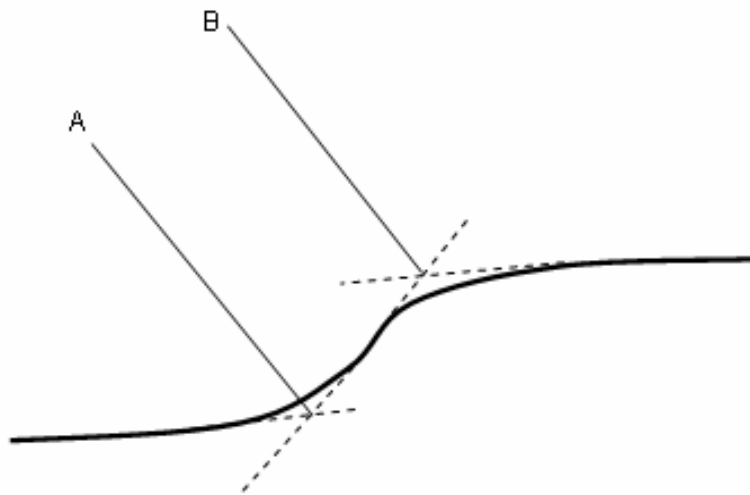


Figure 28 Temperature Transitions Measured by Noting Onset & Offset Points

Thermogravimetric Analysis

Thermogravimetric Analysis (TGA) is a method of measuring the thermal stability of polymers (Keattch, C. J. & Dollimore, D., 1975). Polymer samples are weighed on a thermobalance, which is a highly sensitive scale that monitors a sample's weight as the temperature is increased over time. Data is collected and plotted for the sample's weight versus temperature. Weight loss can occur as excess moisture evaporates and, also, when a polymer decomposes as it loses thermal stability (Stevens, M.P., 1999).

Scanning Electron Microscopy

Scanning Electron Microscopy (SEM) is a method used for viewing a specimen surface at high magnifications. Scattered electrons emitted from an electron beam stimulate a response signal to form an image that contains intensified depth with a 3-D effect (Keatch, C. J. & Dollimore, D., 1975). The surface topology can be analyzed for polymers and details can be noted on dispersions such as cracking or blistering on the coatings (Stevens, M. P., 1999). A chemical analysis can also be made on a specimen through SEM. Elements are identified by noting the atomic number that corresponds with wavelengths produced by an x-ray signal (Goldstein, J. I. & Yakowitz, H., 1975).

REFERENCES

- Bentur, A., S. Diamond, & N. S. Berkl. *Steel Corrosion in Concrete*. New York: Chapman and Hall, 1997.
- Berke, Neal S., E. Escalante, C. K. Nmai & D. Whiting. *Corrosion Activity of Steel Reinforced Concrete Structures*. West Conshohocken, PA: ASTM, 1996.
- Bershtein, Vladimir A. & Victor M. Egorov. *Differential Scanning Calorimetry of Polymers: physics, chemistry, analysis, technology*. New York: Ellis Horwood Ltd., 1994.
- Brown, M. C. and Weyers, R. E., "Corrosion Protection Service Life of Epoxy Coated Reinforcing Steel in Virginia Bridge Decks", VTRC 04-CR7, Virginia Transportation Research Council, Charlottesville, VA, September 2003.
http://www.virginiadot.org/vtrc/main/online_reports/pdf/04-cr7.pdf.
- Chang, J. J., W. Yeih, & C. L. Tsai, "Enhancement of Bond Strength for Epoxy-Coated Rebar Using River Sand," *Construction and Building Materials*, v. 16, n. 8 (2002): 465-472.
- Clear, K. C., W. H. Hartt, J. McIntyre, & S. K. Lee, Performance of Epoxy-Coated Reinforcing Steel in Highway Bridges. 1995. Washington, D. C., National Academy Press.
- Cramer, S. D., B. S. Covino, Jr., S. J. Bullard, G. R. Holcomb, J. H. Russell, M. Ziomek-Moroz, Y. P. Virmani, J. T. Butler, F. J. Nelson, & N. G. Thompson, "Prevention of Chloride-Induced Corrosion Damage to Bridges," *ISIJ International*, v. 42, n. 12 (2002): 1376-1385.
- Crane, Alan P. *Corrosion of Reinforcement in Concrete Construction*. London: Ellis Horwood Limited, 1983.
- Darwin, A. B. & J. D. Scantlebury, "Retarding of Corrosion Processes on Reinforcement Bar in Concrete with FBE Coating," *Cement and Concrete Composites*, v. 24, n. 1 (2002): 73-78.
- Erdogdu, S., T. W. Bremner, & I. L. Kondratova, "Accelerated Testing of Plain and Epoxy-Coated Reinforcement in Simulated Seawater and Chloride Solutions," *Cement and Concrete Research*, v. 31, n. 6 (2001): 861-867.
- Galliano, F. & D. Landolt, "Evaluation of Corrosion Protection Properties of Additives for Waterborne Epoxy Coatings on Steel," *Progress in Organic Coatings*, v. 44, n. 3 (2002): 217-225.

- Gileadi, Eliezer. *Electrode Kinetics for Chemists, Chemical Engineers, & Materials Scientists*. Israel: VHC Publishers, 1993.
- Goldstein, Joseph I. & H. Yakowitz. *Practical Scanning Electron Microscopy: Electron & Ion Microprobe Analysis*. New York, NY: Plenum Press, 1975.
- Hayat, M. A. *Principles and Techniques of Scanning Electron Microscopy*, Union, NJ: Van Nostrand Reinhold Company, 1974.
- Jones, Benny A. *Principles and Prevention of Corrosion*. 2nd Ed. Upper Saddle River, NJ: Prentice Hall, 1996.
- Keatch, C. J. & D. Dollimore. *An Introduction to Thermogravimetry*. 2nd Ed. New York, NY: Heyden & Son Ltd., 1975.
- Leidheler, Henry. *Corrosion Control by Organic Coatings*. Houston: NACE, 1981.
- Mathot, Vincent B. F. *Calorimetry and Thermal Analysis of Polymers*. Munich, NY: Hanser Publishers, 1994.
- Matsushima, Iwao, "Effect of Chloride Concentration and pH on Corrosion of Carbon Steel and Stainless Steel Reinforcements," *Corrosion Engineering*, v. 51, n. 10 (2002); 463-466.
- May, Clayton A. *Epoxy Resins: Chemistry and Technology*. 2nd Ed. New York: Marcel Dekker, Inc., 1988.
- Mietz, J., R. Polder, & B. Elsener. *Corrosion of Reinforcement in Concrete: Corrosion Mechanisms and Corrosion Protection*. London: IOM Communications Ltd., 2002.
- Neville, Adam M. *Properties of Concrete*. 4th Ed. Marshfield, MA: Pitman Publishing, 1996.
- Piess, M. & H. De Deurwaerder, "Effect of Coating Stress on Adherence and on Corrosion Prevention," *Progress in Organic Coatings*, v. 43, n. 1-3 (2001): 18-24.
- Pyc, W. A., Weyers, R. E., Weyers, R. M., Mokarem, D. W., Zemajtis, J., Sprinkel, M. M., and Dillard, J. G., Field Performance of Epoxy-Coated Reinforcing Steel in Virginia Bridge Decks. 2000. Charlottesville, VA, Virginia Transportation Research Council.
- Rossiter, Bryant W. & J. F. Hamilton. *Physical Methods of Chemistry: Electrochemical Methods*. 2nd Ed. Rochester, NY: John Wiley & Sons, 1986.
- Schiessl, P. *Corrosion of Steel in Concrete*. New York: Chapman and Hall, 1988.

St. John, D. A., A. B. Poole, & I. Sims. *Concrete Petrography: A Handbook of Investigative Techniques*. New York, NY: John Wiley & Sons, 1998.

Stevens, Malcolm P. *Polymer Chemistry: an Introduction*. 3rd Ed. New York: Oxford University Press, 1999.

Vedalakshmi, R., K. Kumar, V. Raju, & N. S. Rengaswamy, "Effect of Prior Damage on the Performance of Cement Based Coatings on Rebar: Macrocell Corrosion Studies," *Cement and Concrete Composites*, v. 22, n. 6 (2000): 417-421.

Zivica, V., "Significance and Influence of the Ambient Temperature as a Rate Factor of Steel Reinforcement Corrosion," *Bulletin of Materials Science*, v. 25, n. 5 (2002): 375-379.

VITA

Megan Caroline Wheeler was born in Williamsburg, Virginia on December 17, 1978 to parents, Ronald Charles and Barbara Anne Wheeler. She grew up in Williamsburg and graduated from Lafayette High School in 1997.

Megan attended the University of Virginia where she earned a Bachelor of Arts degree in Physics in May 2001. While attending the University, she spent a summer internship working at the Virginia Transportation Research Council and, in her final academic year, concentrated in civil engineering. During the summer of 2001, Megan worked for CTI Consultants, which is headquartered in Chantilly, Virginia, as a construction inspector.

Megan pursued her Masters of Science degree in Civil Engineering at Virginia Tech where she conducted graduate research on the corrosion protection service life of epoxy coated reinforcement. She graduated from Virginia Tech on December 19, 2003.